Lyman continuum leakage from low-mass galaxies with $M_\star < 10^8\,\mathrm{M}_\odot$

Y. I. Izotov [1]★ G. Worseck [2] D. Schaerer,[3,4] N. G. Guseva,[1] J. Chisholm [5] T. X. Thuan,[6]
K. J. Fricke[7] and A. Verhamme[3]

[1]*Bogolyubov Institute for Theoretical Physics, National Academy of Sciences of Ukraine, 14-b Metrolohichna str., Kyiv UA-03143, Ukraine*
[2]*Institut für Physik und Astronomie, Universität Potsdam, Karl-Liebknecht-Str. 24/25, D-14476 Potsdam, Germany*
[3]*Observatoire de Genève, Université de Genève, 51 Ch. des Maillettes, CH-1290 Versoix, Switzerland*
[4]*IRAP/CNRS, 14, Av. E. Belin, F-31400 Toulouse, France*
[5]*Astronomy Department, University of Texas at Austin, 2515 Speedway, Stop C1400 Austin, TX 78712-1205, USA*
[6]*Astronomy Department, University of Virginia, P.O. Box 400325, Charlottesville, VA 22904-4325, USA*
[7]*Institut für Astrophysik, Göttingen Universität, Friedrich-Hund-Platz 1, D-37077 Göttingen, Germany*

ABSTRACT

We present observations with the Cosmic Origins Spectrograph onboard the *Hubble Space Telescope* of nine low-mass star-forming galaxies at redshifts, z, in the range 0.3179–0.4524, with stellar masses $M_\star < 10^8\,\mathrm{M}_\odot$ and very high specific star-formation rates sSFR $\sim$150–630 Gyr^{-1}, aiming to study the dependence of leaking Lyman continuum (LyC) emission on stellar mass and some other characteristics of the galaxy. We detect LyC emission in four out of nine galaxies with escape fractions, $f_{\rm esc}$(LyC), in the range of 11–35 per cent, and establish upper limits for $f_{\rm esc}$(LyC) in the remaining five galaxies. We observe a narrow Lyα emission line with two peaks in seven galaxies and likely more complex Lyα profiles in the two remaining galaxies. The velocity separation between the peaks $V_{\rm sep}$ varies in the range from $\sim$229 to $\sim$512 km s^{-1}. Our additional data on low-mass galaxies confirm and strengthen the tight anticorrelation between $f_{\rm esc}$(LyC) and $V_{\rm sep}$ found for previous low-redshift galaxy samples with higher stellar masses. $V_{\rm sep}$ remains the best indirect indicator of LyC leakage. It is better than O$_{32}$ on which $f_{\rm esc}$(LyC) depends weakly, with a large scatter. Finally, contrary to expectations, we find no increase of $f_{\rm esc}$(LyC) with decreasing galaxy stellar mass $M_\star$.

Key words: galaxies: abundances – galaxies: dwarf – galaxies: fundamental parameters – galaxies: ISM – galaxies: starburst – dark ages, reionization, first stars.

1 INTRODUCTION

The nature of the main contributors to the reionization of the Universe at redshift $z \gtrsim 6$ is still unknown. Two main types of objects have been proposed, active galactic nuclei (Madau & Haardt 2015) and star-forming galaxies (SFGs) (e.g. Stark 2016, and references therein). Several recent studies (Mitra, Ferrara & Choudhury 2013; Hassan et al. 2018; Matsuoka et al. 2018; Mitra, Choudhury & Ferrara 2018; Kulkarni, Worseck & Hennawi 2019; Wang et al. 2019; Shen et al. 2020) have found that the contribution of active galactic nuclei (AGNs) is small. It has been generally thought that, at high redshifts, numerous faint low-mass SFGs were responsible for the bulk of the ionizing radiation (Ouchi et al. 2009; Wise & Cen 2009; Yajima, Choi & Nagamine 2011; Mitra, Ferrara & Choudhury 2013; Bouwens et al. 2015; Finkelstein et al. 2019; Lewis et al. 2020), whereas the number of relatively bright SFGs is insufficient to fully ionize the Universe (Steidel, Pettini & Adelberger 2001; Cowie, Barger & Trouille 2009; Iwata et al. 2009; Robertson et al. 2013). However, recently Naidu et al. (2020), based on an empirical model of reionization have found that 5 per cent of bright galaxies

with $M_{\rm FUV} < -18$ mag and stellar masses $M_\star/\mathrm{M}_\odot > 10^8$ contribute $\gtrsim$80 per cent of the ionizing luminosity, whereas lower mass galaxies have a minor effect. On the other hand, Meyer et al. (2020), based on the correlation of foreground galaxies with the intergalactic medium (IGM) transmission towards background QSO at the end of reionization, found that a contribution from faint galaxies is necessary to reproduce the observed decreasing IGM opacity and that reionization might be driven by different subpopulations of Lyman-break galaxies (LBGs) and Lyman-alpha emitters (LAEs) at $z \sim 6$.

Additional conditions for galaxies to reionize the Universe require that the escape fraction of their Lyman continuum (LyC) is of the order of 10–20 per cent or higher (e.g. Ouchi et al. 2009; Robertson et al. 2013; Dressler et al. 2015; Robertson et al. 2015; Khaire et al. 2016) and that the ionizing photon production is $\xi_{\rm ion} \sim 10^{25.2}$ Hz erg^{-1} (e.g. Robertson et al. 2013). One of the differences between these studies and the one by Naidu et al. (2020) is that the former authors assume a constant $f_{\rm esc}$(LyC), whereas the latter allowed $f_{\rm esc}$(LyC) to scale with various galaxy properties, e.g. SFR surface density and stellar mass. Finkelstein et al. (2019) looked at how variations in the galaxy properties can translate into different reionization histories. Specifically, they found that variations in the $\xi_{\rm ion}$ strongly favour low mass galaxies as the source of reionization with $f_{\rm esc}$(LyC) values as low as 5 per cent. Thus, scaling relations with

★ E-mail: yizotov@bitp.kiev.ua

galaxy properties are highly uncertain and adopting different ones can completely change the reionization history of the Universe. Studying these limitations, e.g. how the escape fraction of the ionizing radiation depends on the galaxy's stellar mass, is among the main motivations of this study.

The most reliable LyC leakers detected at high redshifts thus far appear to fulfill the condition that $f_{esc}(LyC) \gtrsim 10-20$ per cent. They are the objects *Ion2* ($z = 3.212$; Vanzella et al. 2015; de Barros et al. 2016) with a relative escape fraction $f_{esc}^{rel}(LyC) = 64$ per cent, Q1549-C25 ($z = 3.212$; Shapley et al. 2016) with $f_{esc}(LyC) > 51$ per cent, A2218-Flanking ($z \approx 2.5$; Bian et al. 2017) with $f_{esc}(LyC) > 28-57$ per cent, *Ion3* ($z \approx 4.0$; Vanzella et al. 2018) with $f_{esc}(LyC) \sim 60$ per cent, *Sunburst Arc* ($z \approx 2.37$; Rivera-Thorsen et al. 2019) with $f_{esc}(LyC) \sim 20$ per cent, a $z \sim 1.4$ galaxy with $f_{esc}(LyC) > 20$ per cent (Saha et al. 2020), two $z \geq 3.5$ galaxies with $f_{esc}(LyC) \sim 5-73$ per cent (Meštric et al. 2020) and two GRB galaxies at $z \sim 3$ with $f_{esc}(LyC) \sim 35$ and 8 per cent (Vielfaure et al. 2020). Recently, Fletcher et al. (2019) have shown that fifteen $z \sim 3.1$ LyC leakers have escape fractions ranging from 2 per cent to 82 per cent. Marchi et al. (2017, 2018) and Steidel et al. (2018) report LyC detection in stacked spectra of $z \sim 3$ spectra, after careful removal of possible interlopers with the help of *HST* imaging.

Thus, a small sampling of galaxies near the peak of cosmic star formation history empirically shows that galaxies can emit sufficient ionizing photons to reionize the high-redshift Universe.

Direct observations of high-redshift galaxies are difficult for several reasons, including their faintness, the increase of IGM opacity, and contamination by lower redshift interlopers (e.g. Vanzella et al. 2010, 2012; Inoue et al. 2014; Grazian et al. 2016). Therefore, it is important to identify and study local proxies of this galaxy population. It has been argued that low-mass compact galaxies at low redshifts $z < 1$ with very active star formation may be promising candidates for escaping ionizing radiation (Jaskot & Oey 2013; Nakajima & Ouchi 2014). Low-redshift galaxies, because of their proximity, can be studied in more detail than high-redshift ones and their $f_{esc}(LyC)$ can be derived with a higher reliability. In particular, the intrinsic LyC flux produced by hot stars in a low-redshift galaxy can directly be derived from the observable H β flux, and together with the observed LyC flux, allows the direct determination of $f_{esc}(LyC)$. This technique, which is not possible for most of high-redshift galaxies because of the unobservable H β emission, has been applied in particular by Izotov et al. (2016a,b, 2018a,b).

The general characteristic of compact SFGs is the presence of strong emission lines in the optical spectra of their H II regions, powered by numerous O-stars, which produce plenty of ionizing radiation. Different subsets of compact SFGs, depending on redshift, photometric characteristics, and luminosities, have been variously called 'blue compact dwarf' (BCD) galaxies (e.g. Thuan & Martin 1981; Izotov, Thuan & Lipovetsky 1994; Izotov et al. 2018c), 'blueberry' galaxies (Yang et al. 2017b), 'green pea' (GP) galaxies (Cardamone et al. 2009), or 'luminous compact' star-forming galaxies (LCGs) (Izotov, Guseva & Thuan 2011).

Stellar masses, star formation rates (SFR), and metallicities of compact SFGs vary in wide ranges and they are similar to those of high-redshift SFGs including Ly α emitting galaxies (Izotov et al. 2015). Many low-redshift compact SFGs are characterized by high line ratios $O_{32} = [O III]\lambda5007/[O II]\lambda3727 \gtrsim 4-5$, reaching values of up to 60 in some galaxies (Stasińska et al. 2015). These high values are not yet observed in high-z galaxies, However, their *Spitzer* colours suggest strong [O III] + H β equivalent widths (Labbé et al. 2013; Smit et al. 2014; de Barros et al. 2019; Endsley et al. 2021). Such high values may indicate that the ISM is predominantly ionized,

allowing the escape of Lyman continuum photons (Jaskot & Oey 2013; Nakajima & Ouchi 2014). Indeed, Izotov et al. (2016a,b, 2018a,b) obtained *HST*/COS observations of eleven compact SFGs at redshifts $z \sim 0.3-0.4$ and with $O_{32} = 5-28$ and $M_{\star} \sim 6 \times 10^7 - 6 \times 10^9$ $M_{\odot}$, and found all these galaxies to be leaking LyC radiation, with an escape fraction in the range of 2–72 per cent. We note that recent X-shooter observations of one of the strong high-z leakers, *Ion2*, reveal the emission-line characteristics in the optical range to be similar to those of $\sim 0.3-0.4$ LyC leakers, in particular, a high $O_{32} \sim 9$ (Vanzella et al. 2020). Furthermore, the Ly α profile of ten galaxies shows a double peak with one having a triple peak. All these profiles show a small velocity separation of the peaks (< 450 km s^{-1}), as predicted by Verhamme et al. (2015) for low H I column densities.

Finally, an analysis of UV absorption lines, including hydrogen lines of the Lyman series and heavy element lines such as Si II $\lambda1260$ can provide a consistent and accurate measure of the Lyman continuum escape fraction (e.g. Chisholm et al. 2018; Gazagnes et al. 2018; Gazagnes et al. 2020). Mg II $\lambda2796$, 2803 emission provides also a strong constraint of the LyC escape and the doublet ratio can be used to infer the neutral gas column density (Henry et al. 2018; Chisholm et al. 2020).

The goal of this paper is to determine $f_{esc}(LyC)$ for nine low-mass galaxies with $M_{\star} < 10^8$ $M_{\odot}$. We wish to extend the range of stellar masses down to 10^7 $M_{\odot}$ as high-redshift galaxies, at the epoch of reionization, are thought to be low-mass objects. We also wish to enlarge the known sample of low-redshift LyC leakers and to search for reliable diagnostics for the indirect determination of $f_{esc}(LyC)$.

Izotov et al. (2018b) using the sample of known low-redshift LyC leakers have considered three indicators for diagnostics, the velocity separation V_{sep} between the Ly α peaks, the O_{32} ratios, and the stellar mass $M_{\star}$. They have found a tight anticorrelation between $f_{esc}(LyC)$ and V_{sep}, making V_{sep} one of the best indirect indicators for escaping ionizing radiation.

As mentioned before, a high O_{32} ratio has been suggested to be a promising indirect indicator of escaping LyC emission in galaxies at any redshift. Although Izotov et al. (2018b) and Nakajima et al. (2020) did find some trend of increasing $f_{esc}(LyC)$ with increasing O_{32}, the dependence is weak, with a large scatter.

It has also been suggested that $f_{esc}(LyC)$ tends to be higher in low-mass galaxies (Wise et al. 2014; Trebitsch et al. 2017). Stellar masses, $M_{\star}$, are available for a large number of SFGs because ground-based observations are sufficient for their determination. Izotov et al. (2018b) found only a relatively weak anticorrelation between $f_{esc}(LyC)$ and $M_{\star}$. However, this conclusion is based mostly on objects with $M_{\star} \geq 10^8$ $M_{\odot}$, with the exception of one galaxy. Intriguingly, the unique galaxy in the LyC leaker sample with a stellar mass $< 10^8$ $M_{\odot}$, J1243+4646, is also the one with the highest $f_{esc}(LyC)$, equal to 72 per cent. The question then arises: are lower mass compact galaxies stronger LyC leakers?

Fletcher et al. (2019) have found more LyC leakers at $z \sim 3.1$ with $M_{\star} < 10^8$ $M_{\odot}$. However, they derived $M_{\star}$ from UV rest-frame photometry, which is dominated by the radiation from hot massive stars, while the stellar masses of low-redshift LyC leakers are derived from the rest-frame spectra in the optical range which also includes the emission of lower mass cooler stars. Furthermore, the stellar masses derived by Fletcher et al. (2019) are up to 1.5 dex lower than the values derived by Nakajima et al. (2018) for the same galaxies. Therefore, the $M_{\star}$ of Fletcher et al. (2019) might be underestimated.

In this paper, we present new *HST*/COS observations of the LyC in nine compact SFGs, with the lowest $M_{\star} < 10^8$ $M_{\odot}$ ever observed at $z \sim 0.3-0.4$. We wish to detect their ionizing radiation, and examine its behaviour over a wide range of stellar masses. The

properties of the selected SFGs derived from observations in the optical range are presented in Section 2. The *HST* observations and data reduction are described in Section 3. The surface brightness profiles in the UV range are discussed in Section 4. In Section 5, we compare the *HST*/COS spectra with the extrapolation of the modelled SEDs to the UV range. Ly α emission is considered in Section 6. The escaping Lyman continuum emission is discussed in Section 7 together with the corresponding escape fractions. The indirect indicators of escaping LyC emission are considered in Section 8. We summarize our findings in Section 9.

2 PROPERTIES OF SELECTED GALAXIES DERIVED FROM OBSERVATIONS IN THE OPTICAL RANGE

We selected a sample of local compact low-mass SFGs ($M_\star < 10^8 \, \mathrm{M_\odot}$) to observe their Ly α and LyC emission with *HST*/COS. The sources are selected from SDSS in the redshift range $z = 0.32$–0.45, which allows efficient observations of the LyC with COS. They are also chosen to be the brightest and have the highest O_{32} ratios and the highest equivalent widths EW(H β) of the H β emission line so that a galaxy can be acquired and observed with low- and medium-resolution gratings in one visit, consisting of five orbits. These selection criteria yield a total sample of nine galaxies. They are listed in Table 1. The important features of the objects in this sample compared to the previous ones are (1) the lower stellar masses, extending the mass range down to $\sim 2 \times 10^7 \, \mathrm{M_\odot}$, which is more typical of high-z SFGs; (2) the large range of $O_{32} \sim 4$–14, similar to that of the LyC leakers of Izotov et al. (2016a,b, 2018a,b); and (3) the fainter UV absolute magnitudes $M_{\mathrm{FUV}} \sim -19$ to -20 mag, whereas the galaxies in Izotov et al. (2016a,b, 2018a,b) are generally brighter, with $M_{\mathrm{FUV}} \sim -20$ to -21 mag. This is fainter than the characteristic $M_{\mathrm{FUV}} \sim -21$ mag for galaxies at $z \sim 6$. Thus, our galaxies represent the faint end of the luminosity function. It is also worth noting that all objects from the selected sample have low metallicities (the range of oxygen abundances is ~ 7.8–8.1) and high equivalent widths of the H β emission line (158–435 Å). All galaxies are nearly unresolved by the SDSS g-band images, which have FWHMs of 1.0–1.6 arcsec, so that all the galaxy's light falls within the 2.5 arcsec diameter COS aperture, ensuring that global quantities can be derived.

The SDSS, *GALEX*, and *WISE* apparent magnitudes of the selected galaxies are shown in Table 2, indicating that these SFGs are among the faintest low-redshift LyC leaker candidates selected for *HST* observations. In fact, only four out of nine galaxies have been detected in the FUV range and only two galaxies are present in the AllWISE catalogue.

To derive absolute magnitudes and other integrated parameters, we adopted luminosity and angular size distances (NASA Extragalactic Database (NED);[1] Wright 2006) with the cosmological parameters $H_0 = 67.1 \, \mathrm{km \, s^{-1} \, Mpc^{-1}}$, $\Omega_\Lambda = 0.682$, $\Omega_m = 0.318$ (Ade et al. 2014). These distances are presented in Table 1.

2.1 Interstellar extinction and element abundances

Internal interstellar extinction has been derived from the observed decrement of all hydrogen emission lines, which are measurable

in the SDSS spectra (Izotov et al. 1994). First, the emission-line fluxes in the observed SDSS spectra, uncorrected for redshift, were corrected for the Milky Way extinction with $A(V)_{\mathrm{MW}}$ from the NED, adopting the Cardelli, Clayton & Mathis (1989) reddening law and $R(V)_{\mathrm{MW}} = 3.1$. Secondly, the fluxes of emission lines at the rest-frame wavelengths were corrected for the internal extinction of galaxies with $R(V)_{\mathrm{int}} = 3.1$ and $A(V)_{\mathrm{int}} = 3.1 \times E(B - V)_{\mathrm{int}}$, where $E(B - V)_{\mathrm{int}} = C(H\beta)_{\mathrm{int}}/1.47$ (Aller 1984). Finally, the extinction-corrected emission lines are used to derive ionic and total element abundances following the methods described in Izotov et al. (2006) and Guseva et al. (2013).

The emission-line fluxes $I(\lambda)$ relative to the H β flux corrected for both the Milky Way and internal extinctions, the rest-frame equivalent widths, the Milky Way ($C(H\beta)_{\mathrm{MW}}$) and internal ($C(H\beta)_{\mathrm{int}}$) extinction coefficients, and extinction-corrected H β fluxes are shown in Table 3. We note that H α emission lines in SDSS spectra of two galaxies, J0232$-$0426 and J1046+5827 are clipped and therefore their fluxes are lower than the theoretical recombination values. Consequently, we excluded these lines from the determination of internal extinctions in J0232$-$0426 and J1046+5827. The fluxes and the direct T_e method are used to derive the physical conditions (electron temperature and electron number density) and the element abundances in the H II regions. These quantities are shown in Table 4. The oxygen abundances are comparable to those in known low-redshift LyC leakers by Izotov et al. (2016a,b, 2018a,b). The ratios of the α-element (neon and magnesium) abundances to oxygen abundance are similar to those in dwarf emission-line galaxies (e.g. Izotov et al. 2006; Guseva et al. 2013). On the other hand, the nitrogen-to-oxygen abundance ratios in some galaxies are somewhat elevated, similar to those in other LyC leakers at $z \gtrsim 0.3$.

2.2 Absolute magnitudes, H β luminosities, and stellar masses

For absolute FUV magnitudes, we do not use the observed *GALEX* FUV apparent magnitudes for two reasons: (1) only four galaxies are detected by *GALEX* in the FUV range; (2) for the remaining galaxies, FUV magnitudes are given for emission at somewhat different wavelengths. Therefore, for homogeneity, we derive absolute magnitudes from the fluxes of the extinction-corrected spectral distribution (SED) at the rest-frame wavelength $\lambda = 1500$ Å. We designate these absolute magnitudes as M_{FUV}. They are, on average, ~ 0.7 mag fainter than M_{FUV}s for other $z \sim 0.3$–0.4 LyC leakers.

The H β luminosity $L(H\beta)$ and the corresponding star-formation rates SFR were obtained from the extinction-corrected H β fluxes, using the relation of Kennicutt (1998) for the SFR. SFRs are increased by a factor $1/[1 - f_{\mathrm{esc}}(\mathrm{LyC})]$ to take into account the escaping ionizing radiation which is discussed later. The SFRs corrected for escaping LyC radiation are shown in Table 5. They are somewhat below the range of 14–80 $\mathrm{M_\odot \, yr^{-1}}$ for the other LyC leakers studied by Izotov et al. (2016a,b, 2018a,b), presumably because of their smaller stellar masses. On the other hand, their specific star formation rates, sSFR = SFR/$M_\star$, are >150 $\mathrm{Gyr^{-1}}$, with the highest value of $\sim 630 \, \mathrm{Gyr^{-1}}$ for J1121+3806, which has also the lowest stellar mass (Table 5). These sSFR are among the largest sSFR for dwarf SFGs at any redshift and they are significantly higher than the sSFRs observed in other LyC leakers (Izotov et al. 2016a,b, 2018a,b).

We use the SDSS spectra of our LyC leakers to fit the SED and derive their stellar masses. The fitting method, using a two-component model, is described in Izotov et al. (2018a,b). Spectral energy distributions of instantaneous bursts in the range between 0 and 10 Gyr with evolutionary tracks of non-rotating stars by Girardi et al. (2000) and a combination of stellar atmosphere models

---

[1]NASA/IPAC Extragalactic Database (NED) is operated by the Jet Propulsion Laboratory, California Institute of Technology, under contract with the National Aeronautics and Space Administration.

Table 1. Coordinates, redshifts, distances, oxygen abundances, and O_{32} ratios of selected galaxies.

Name	R.A.(2000.0)	Dec.(2000.0)	z	$D_L y^a$	D_A^b	12+logO/H^c	O_{32}^c
J0232−0426	02:32:16.09	−04:26:26.72	0.45236	2539	1204	7.88	14.2
J0919+4906	09:19:55.78	+49:06:08.75	0.40512	2227	1128	7.77	11.5
J1046+5827	10:46:01.98	+58:27:56.95	0.39677	2172	1114	8.01	4.7
J1121+3806	11:21:18.22	+38:06:42.80	0.31788	1675	965	7.96	7.3
J1127+4610	11:27:21.00	+46:10:42.49	0.32230	1702	974	7.84	6.0
J1233+4959	12:33:30.78	+49:59:49.45	0.42194	2337	1156	8.11	11.0
J1349+5631	13:49:55.10	+56:31:10.90	0.36366	1960	1054	7.91	4.0
J1355+1457	13:55:53.46	+14:57:01.48	0.36513	1970	1057	7.77	6.1
J1455+6107	14:55:59.57	+61:07:19.70	0.36793	1987	1062	7.91	4.1

Notes. ^{a}Luminosity distance in Mpc (NED; Wright 2006).
^{b}Angular size distance in Mpc (NED; Wright 2006).
^{c}Derived in this paper from the SDSS spectrum.

Table 2. Apparent AB magnitudes with errors in parentheses compiled from the SDSS and *GALEX* data bases and apparent Vega magnitudes from the *WISE* data base.

Name	SDSS					*GALEX*		*WISE*			
	u	g	r	i	z	FUV	NUV	W1	W2	W3	W4
	(err)	(err)	(err)	(err)	(err)	(err)	(err)	(err)	(err)	(err)	(err)
J0232−0426	23.38	22.13	21.93	20.85	21.59	...	21.26	...	...	...	...
	(0.73)	(0.11)	(0.11)	(0.06)	(0.45)	(...)	(0.09)	(...)	(...)	(...)	(...)
J0919+4906	22.33	21.97	21.95	20.78	22.32	22.54	21.92	...	...	...	...
	(0.27)	(0.08)	(0.10)	(0.06)	(0.62)	(0.21)	(0.12)	(...)	(...)	(...)	(...)
J1046+5827	21.20	21.07	21.23	20.55	20.57	21.30	21.02	17.70	...	...	...
	(0.09)	(0.04)	(0.06)	(0.05)	(0.16)	(0.03)	(0.02)	(0.18)	(...)	(...)	(...)
J1121+3806	22.18	22.05	21.19	22.75	21.19	...	...	...	...	...	...
	(0.17)	(0.07)	(0.05)	(0.28)	(0.26)	(...)	(...)	(...)	(...)	(...)	(...)
J1127+4610	21.97	22.31	21.63	23.31	21.63	...	22.22	...	...	...	...
	(0.21)	(0.11)	(0.11)	(0.61)	(0.52)	(...)	(0.39)	(...)	(...)	(...)	(...)
J1233+4959	21.70	21.92	21.90	20.80	21.48	...	21.91	...	...	...	...
	(0.16)	(0.08)	(0.11)	(0.06)	(0.41)	(...)	(0.12)	(...)	(...)	(...)	(...)
J1349+5631	22.48	22.45	22.08	23.00	22.25	22.24	22.14	17.96	16.89	...	...
	(0.29)	(0.11)	(0.11)	(0.38)	(0.61)	(0.36)	(0.32)	(0.19)	(0.27)	(...)	(...)
J1355+1457	22.05	21.62	21.40	21.66	20.73	...	21.13	...	...	...	...
	(0.15)	(0.05)	(0.05)	(0.09)	(0.14)	(...)	(0.10)	(...)	(...)	(...)	(...)
J1455+6107	21.84	21.51	21.33	21.37	21.56	21.52	21.70	...	...	...	...
	(0.17)	(0.05)	(0.07)	(0.10)	(0.39)	(0.39)	(0.39)	(...)	(...)	(...)	(...)

(Schmutz, Leitherer & Gruenwald 1992; Lejeune, Buser & Cuisiner 1997) are used to produce the integrated SED for each galaxy. The adoption of other sets of evolutionary tracks of rotating and non-rotating stars and stellar atmosphere models would, in particular, change the level of Lyman continuum by ∼10 per cent at most (Izotov et al. 2016a). The star formation history is approximated by a young burst with a randomly varying age t_b in the range < 10 Myr, and a continuous star formation for older ages between times t_1 and t_2, randomly varying in the range 10 Myr–10 Gyr, and adopting a constant SFR. The contribution of the two components is determined by randomly varying the ratio of their stellar masses, $b = M_o/M_y$, in the range 0.1–1000, where M_o and M_y are the masses of the old and young stellar populations.

The nebular continuum emission, including free–free and free–bound hydrogen and helium emission, and two-photon emission, is also taken into account using the observed H β flux, the ISM temperature and density. The fraction of nebular emission in the observed continuum near H β is determined by the ratio of the observed H β equivalent width EW(H β)$_{obs}$, reduced to the rest frame, to the equivalent EW(H β)$_{rec}$ for pure nebular emission. EW(H β)$_{rec}$ varies from ∼900 to ∼1100 Å, for electron temperatures in the range $T_e = 10\,000–20\,000$ K. For example, the fraction of nebular continuum near H β in J0919+4906 with EW(H β)$_{obs} =$ 435 Å (Table 3) is ∼40 per cent and the remaining 60 per cent of emission in the continuum is stellar. We note that non-negligible nebular emission, including both the continuum and emission lines, is produced only by the burst.

The Salpeter initial mass function (IMF) is adopted, with a slope of −2.35, upper and lower mass limits M_{up} and M_{low} of 100 M$_\odot$ and 0.1 M$_\odot$, respectively. A χ^2 minimization technique was used (1) to fit the continuum in such parts of the wavelength range 3600–6500 Å, where the SDSS spectrum is least noisy and free of nebular emission lines, and (2) to reproduce the observed H β and H α equivalent widths.

To illustrate the quality of our SED fitting, Fig. 1 shows the modelled stellar, nebular, and total SEDs superposed upon the rest-frame extinction-corrected SDSS spectra. For all galaxies we find good agreement. The masses of young (M_y) and old (M_o) stellar populations, and total stellar masses ($M_\star = M_y + M_o$) of our LyC leakers derived from SED fitting are presented in Table 5. They are derived in exactly the same way as the stellar masses for the other LyC leakers studied by our team (Izotov et al. 2016a,b, 2018a,b), permitting a direct comparison. They are considerably lower, being all less than 10^8 M$_\odot$.

Table 3. Extinction-corrected fluxes and rest-frame equivalent widths of the emission lines in SDSS spectra.

		Galaxy									
Line	λ	J0232−0426		J0919+4906		J1046+5827		J1121+3806		J1127+4610	
		I^a	EW^b	I^a	EW^b	I^a	EW^b	I^a	EW^b	I^a	EW^b
Mg II	2796	15.8 ± 4.7	10	25.8 ± 6.7	19	29.6 ± 4.6	11	20.7 ± 4.1	10	34.4 ± 8.0	26
Mg II	2803	14.9 ± 4.7	9	19.2 ± 6.3	14	23.8 ± 4.3	9	15.3 ± 3.6	10	12.4 ± 6.6	10
[O II]	3727	44.5 ± 6.9	68	55.0 ± 4.6	127	130.6 ± 8.9	101	83.6 ± 6.8	130	89.3 ± 16.	72
H12	3750	3.8 ± 3.8	5	4.2 ± 1.5	17	5.6 ± 4.7	4	...	...	...	...
H11	3771	5.0 ± 4.3	6	7.6 ± 2.0	21	7.0 ± 5.5	4	...	...	...	...
H10	3798	6.9 ± 3.6	14	6.7 ± 2.1	20	7.6 ± 4.5	7	...	...	...	...
H9	3836	11.1 ± 4.1	21	9.7 ± 1.9	28	13.0 ± 4.6	19	10.3 ± 3.6	16	12.2 ± 7.4	13
[Ne III]	3869	37.4 ± 6.5	46	54.2 ± 4.5	153	51.1 ± 5.3	40	49.1 ± 5.1	88	43.2 ± 11.	49
H8+He I	3889	17.8 ± 5.5	23	25.3 ± 3.3	55	21.2 ± 6.3	15	19.4 ± 4.8	87	28.5 ± 9.0	40
H7+[Ne III]	3969	30.3 ± 6.7	40	33.0 ± 3.5	96	37.3 ± 6.0	38	34.9 ± 5.1	60	33.3 ± 9.7	51
Hδ	4101	28.3 ± 5.7	87	22.6 ± 2.9	71	32.3 ± 5.4	39	28.9 ± 4.8	51	29.3 ± 9.5	37
Hγ	4340	40.5 ± 7.5	54	45.4 ± 4.2	118	47.6 ± 6.0	66	47.0 ± 5.2	94	50.8 ± 12.	72
[O III]	4363	12.3 ± 4.3	17	15.3 ± 2.6	44	9.7 ± 2.8	11	10.2 ± 2.7	19	10.0 ± 6.3	16
He I	4471	6.4 ± 2.9	18	...	...	...	...	4.8 ± 2.3	7	...	...
Hβ	4861	100.0 ± 11.	227	100.0 ± 6.5	435	100.0 ± 8.2	170	100.0 ± 8.1	317	100.0 ± 17.	158
[O III]	4959	219.6 ± 16.	480	209.9 ± 10.	992	199.6 ± 11.	358	212.6 ± 12.	703	169.8 ± 23.	201
[O III]	5007	632.4 ± 35.	1977	635.0 ± 22.	2547	613.4 ± 23.	1116	616.2 ± 23.	2222	531.7 ± 45.	685
He I	5876	10.6 ± 4.2	37	10.4 ± 2.4	69	12.0 ± 3.0	67	...	...	...	...
Hα	6563	255.6 ± 23.^{c}	472	279.2 ± 14.	2250	259.1 ± 16.^{c}	851	274.5 ± 17.	901	273.8 ± 33.	1038
[N II]	6583	...	...	7.3 ± 2.0	76	5.3 ± 2.8	15	6.1 ± 2.4	36	...	...
[S II]	6717	...	...	...	...	...	...	...	...	...	...
[S II]	6731	...	...	...	...	...	...	...	...	...	...
C(Hβ)$_{int}$^{d}		0.050 ± 0.109		0.075 ± 0.061		0.050 ± 0.074		0.050 ± 0.074		0.050 ± 0.156	
C(Hβ)$_{MW}$^{e}		0.029		0.020		0.011		0.028		0.025	
EW(Hβ)^b		227 ± 26		435 ± 26		170 ± 40		317 ± 34		158 ± 26	
I(Hβ)^f		4.4 ± 0.5		5.1 ± 0.4		8.8 ± 0.7		7.9 ± 0.6		4.8 ± 0.8	

		Galaxy									
Line	λ	J1233+4959		J1349+5631		J1355+1457		J1455+6107		–	–
		I^a	EW^b	I^a	EW^b	I^a	EW^b	I^a	EW^b	–	–
Mg II	2796	17.6 ± 3.5	10	12.7 ± 4.7	14	32.9 ± 7.2	28	32.2 ± 6.2	13	–	–
Mg II	2803	9.6 ± 3.0	4	15.1 ± 5.2	9	34.8 ± 7.4	15	11.6 ± 4.9	11	–	–
[O II]	3727	60.8 ± 5.9	66	144.8 ± 13.	158	100.5 ± 4.8	162	140.2 ± 6.5	212	–	–
H12	3750	...	...	...	...	4.1 ± 1.2	7	...	...	–	–
H11	3771	...	...	...	...	4.4 ± 1.4	8	...	...	–	–
H10	3798	...	...	...	...	8.1 ± 1.6	16	6.3 ± 1.5	11	–	–
H9	3836	...	...	...	...	8.9 ± 1.6	23	10.5 ± 1.8	21	–	–
[Ne III]	3869	51.4 ± 5.4	46	47.9 ± 7.2	98	49.5 ± 3.3	61	54.1 ± 3.8	78	–	–
H8+He I	3889	20.2 ± 4.5	26	23.6 ± 6.5	43	21.5 ± 2.2	36	28.1 ± 2.8	47	–	–
H7+[Ne III]	3969	31.3 ± 5.4	39	28.9 ± 8.2	35	31.4 ± 2.7	51	28.1 ± 2.8	47	–	–
Hδ	4101	27.9 ± 4.6	49	22.9 ± 5.4	55	28.5 ± 2.4	86	27.5 ± 2.9	67	–	–
Hγ	4340	50.5 ± 6.0	80	44.1 ± 8.1	77	47.0 ± 3.1	117	48.3 ± 4.1	157	–	–
[O III]	4363	8.5 ± 2.6	11	10.9 ± 3.9	13	15.3 ± 1.9	41	11.3 ± 1.7	29	–	–
He I	4471	...	...	...	...	...	...	3.9 ± 1.3	7	–	–
Hβ	4861	100.0 ± 7.9	305	100.0 ± 12.	172	100.0 ± 4.8	265	100.0 ± 5.3	278	–	–
[O III]	4959	223.7 ± 12.	542	190.2 ± 16.	450	202.7 ± 7.4	597	193.1 ± 7.8	747	–	–
[O III]	5007	667.2 ± 25.	1424	579.4 ± 32.	1649	614.3 ± 16.	1714	578.4 ± 17.	2049	–	–
He I	5876	...	...	16.1 ± 4.9	47	11.3 ± 1.8	59	9.8 ± 2.0	26	–	–
Hα	6563	275.1 ± 17.	1469	282.6 ± 24.	1326	280.6 ± 11.	1851	281.9 ± 12.	839	–	–
[N II]	6583	11.6 ± 3.1	59	7.5 ± 4.1	10	...	...	...	...	–	–
[S II]	6717	...	...	17.5 ± 5.6	41	7.5 ± 1.7	49	7.3 ± 2.0	18	–	–
[S II]	6731	...	...	13.0 ± 5.0	32	5.6 ± 1.6	35	8.5 ± 2.1	21	–	–
C(Hβ)$_{int}$^{d}	–	0.050 ± 0.073		0.110 ± 0.100		0.135 ± 0.045		0.090 ± 0.050		–	–
C(Hβ)$_{MW}$^{e}	–	0.023		0.013		0.028		0.018		–	–
EW(Hβ)^b	–	305 ± 30		172 ± 36		265 ± 12		278 ± 10		–	–
I(Hβ)^f	–	8.7 ± 0.7		5.0 ± 0.5		12.8 ± 0.6		8.7 ± 0.4		–	–

Notes. ^{a} $I = 100 \times I(\lambda)/I(H\beta)$, where $I(\lambda)$ and $I(H\beta)$ are fluxes of emission lines, corrected for both the Milky Way and internal extinction.
^{b}Rest-frame equivalent width in Å.
^{c}Clipped line.
^{d}Internal galaxy extinction coefficient.
^{e}Milky Way extinction coefficient from the NED.
^{f}Extinction-corrected flux but not corrected for f_{esc}(LyC), in 10^{-16} erg s^{-1} cm^{-2}.

Table 4. Electron temperatures, electron number densities, and element abundances in H II regions.

Galaxy	J0232−0426	J0919+4906	J1046+5827	J1121+3806	J1127+4610
T_e ([O III]), K	14980 ± 2380	16660 ± 1440	13780 ± 1680	14010 ± 1580	14890 ± 2300
T_e ([O II]), K	13990 ± 2070	14810 ± 1190	13230 ± 1510	13390 ± 1410	13940 ± 1750
N_e ([S II]), cm^{-3}	10 ± 10	10 ± 10	10 ± 10	10 ± 10	10 ± 10
$O^+/H^+ \times 10^5$	0.50 ± 0.12	0.52 ± 0.06	1.78 ± 0.31	1.10 ± 0.18	1.02 ± 0.38
$O^{2+}/H^+ \times 10^5$	7.05 ± 0.48	5.40 ± 0.17	8.36 ± 0.57	8.11 ± 0.49	5.89 ± 0.71
O/H× 10^5	7.55 ± 0.50	5.92 ± 0.18	10.14 ± 0.65	9.20 ± 0.52	6.92 ± 0.81
12+log O/H	7.88 ± 0.03	7.77 ± 0.01	8.01 ± 0.03	7.96 ± 0.02	7.84 ± 0.05
$N^+/H^+ \times 10^6$	...	0.55 ± 0.16	0.51 ± 0.29	0.56 ± 0.24	...
ICF(N)^a	...	10.22	5.41	7.59	...
N/H× 10^6	...	5.62 ± 1.86	2.74 ± 1.63	4.28 ± 1.99	...
log N/O	...	−1.02 ± 0.14	−1.57 ± 0.26	−1.33 ± 0.20	...
$Ne^{2+}/H^+ \times 10^5$	1.00 ± 0.24	1.08 ± 0.11	1.77 ± 0.32	1.61 ± 0.27	1.18 ± 0.46
ICF(Ne)^a	1.01	1.03	1.09	1.04	1.06
Ne/H× 10^5	1.01 ± 0.24	1.11 ± 0.12	1.92 ± 0.35	1.67 ± 0.28	1.25 ± 0.48
log Ne/O	−0.87 ± 0.11	−0.73 ± 0.05	−0.72 ± 0.08	−0.74 ± 0.08	−0.74 ± 0.17
$Mg^+/H^+ \times 10^6$	0.27 ± 0.09	0.32 ± 0.10	0.60 ± 0.15	0.38 ± 0.09	0.42 ± 0.19
ICF(Mg)^a	22.89	19.23	10.47	14.24	12.13
Mg/H× 10^6	6.23 ± 1.96	6.17 ± 1.93	6.31 ± 1.57	5.41 ± 1.32	5.11 ± 2.27
log Mg/O	−1.06 ± 0.14	−1.10 ± 0.14	−1.19 ± 0.11	−1.21 ± 0.11	−1.11 ± 0.20
Galaxy	J1233+4959	J1349+5631	J1355+1457	J1455+6107	–
T_e ([O III]), K	12600 ± 1490	14860 ± 2420	16940 ± 1090	15030 ± 1060	–
T_e ([O II]), K	12340 ± 1380	13920 ± 2120	14920 ± 900	14020 ± 920	–
N_e ([S II]), cm^{-3}	10 ± 10	77 ± 130	76 ± 59	1151 ± 305	–
$O^+/H^+ \times 10^5$	1.06 ± 0.22	1.68 ± 0.35	0.93 ± 0.07	1.78 ± 0.14	–
$O^{2+}/H^+ \times 10^5$	11.75 ± 1.04	6.50 ± 0.47	5.02 ± 0.11	6.33 ± 0.21	–
O/H× 10^5	12.81 ± 1.06	8.18 ± 0.58	5.95 ± 0.13	8.11 ± 0.25	–
12+log O/H	8.11 ± 0.04	7.91 ± 0.03	7.77 ± 0.01	7.91 ± 0.01	–
$N^+/H^+ \times 10^6$	1.29 ± 0.37	0.64 ± 0.37	...	...	–
ICF(N)^a	10.21	4.73	...	...	–
N/H× 10^6	1.31 ± 0.44	3.05 ± 1.83	...	...	–
log N/O	−0.99 ± 0.15	−1.43 ± 0.26	...	...	–
$Ne^{2+}/H^+ \times 10^5$	2.38 ± 0.49	1.32 ± 0.30	0.94 ± 0.08	1.44 ± 0.14	–
ICF(Ne)^a	0.99	1.11	1.07	1.12	–
Ne/H× 10^5	2.37 ± 0.49	1.46 ± 0.33	1.01 ± 0.08	1.61 ± 0.16	–
log Ne/O	−0.73 ± 0.10	−0.75 ± 0.10	−0.77 ± 0.04	−0.70 ± 0.05	–
$Mg^+/H^+ \times 10^6$	0.41 ± 0.12	0.26 ± 0.10	0.47 ± 0.13	0.40 ± 0.12	–
ICF(Mg)^a	19.25	9.55	12.08	8.84	–
Mg/H× 10^6	7.95 ± 2.24	2.51 ± 0.94	5.62 ± 1.58	3.52 ± 1.07	–
log Mg/O	−1.19 ± 0.13	−1.51 ± 0.17	−1.03 ± 0.12	−1.36 ± 0.13	–

Note. ^{a}Ionization correction factor.

We find that the masses of the old stellar population are lower or similar to those of the young stellar population. However, the determination of the mass M_o of the old stellar population is very uncertain because of the strong dominance of the young stellar population in the SDSS optical spectrum. For example, the luminosity of a young stellar population with an age of 3 Myr at the wavelength 5000 Å is ∼250 times higher than the luminosity of an old population with an age of 1 Gyr. Therefore, to have a non-negligible contribution of ∼5 per cent to emission at 5000 Å, the mass of the old stellar population should be ∼10 times that of the young stellar population, corresponding to $b \gtrsim 10$. The SED at lower b is not sensitive to the presence of the old stellar population. On the other hand, the stellar mass of the young stellar population M_y is reliable because it is primarily determined by the Hβ luminosity. We also note that the SFR derived from the Hβ emission line is similar to the value M_y/t_b obtained from our modelled SEDs (see Table 5). However, the derived SFRs and sSFRs are just an indication of the galaxy properties. They are not used for SED fitting and thus have no impact on the determination of the LyC escape fraction.

3 *HST*/COS OBSERVATIONS AND DATA REDUCTION

HST/COS spectroscopy of the nine LyC leaker candidates was obtained in program GO 15639 (PI: Y. I. Izotov) during the period 2019 September–2020 May. The observational details are presented in Table 6. As in our previous programs (Izotov et al. 2016a,b, 2018a,b), the galaxies were directly acquired by COS near ultraviolet (NUV) imaging. The NUV-brightest region of each target was centred in the ∼2.5 arcsec diameter spectroscopic aperture (Fig. 2). Although the galaxies show generally a compact star-forming region superimposed upon an extended low-surface-brightness (LSB) component and, in the case of J0232−0426, several star-forming knots, their sizes are smaller than the central unvignetted 0.8 arcsec diameter region of the spectroscopic aperture (Fisher et al. 2018), except for J0232−0426. However, even for this galaxy more than 90 per cent of the emission is concentrated in the 0.8 arcsec diameter region. Hence, the galaxy quantities derived from the COS spectra do not require corrections for vignetting. We note, however, that the acquisition exposure failed for J1046+5827. Therefore, no acquisition image is available for this

Table 5. Integrated characteristics.

Name	M_{FUV} [a]	$\log M_\star$ [b]	$\log M_y$ [b]	$\log M_o$ [b]	$\log L(H\beta)$ [c]	t_b [d]	SFR [e]	sSFR [f]	α [g]	r_{50} [h]	Σ_1 [i]	Σ_2 [j]
J0232−0426	−19.17	7.49	7.40	6.76	41.53	4.4	7.5	250	0.47	0.13	10.8	141
J0919+4906	−19.15	7.51	7.46	6.57	41.48	2.6	8.4	250	0.59	0.12	6.1	148
J1046+5827	−20.11	7.89	7.84	6.88	41.70	4.8	11.0	160	...[k]	...[k]	...[k]	...[k]
J1121+3806	−18.85	7.20	7.14	6.32	41.42	2.7	10.0	630	0.46	0.16	8.9	73
J1127+4610	−19.00	7.44	7.36	6.66	41.22	4.7	4.2	160	0.52	0.15	4.4	52
J1233+4959	−19.97	7.79	7.57	7.38	41.75	3.3	14.4	250	0.59	0.17	11.5	139
J1349+5631	−18.76	7.36	7.29	6.58	41.36	4.7	5.1	200	0.39	0.19	10.7	45
J1355+1457	−19.96	7.74	7.61	7.13	41.77	3.6	13.1	250	0.34	0.21	36.0	95
J1455+6107	−19.77	7.90	7.54	7.65	41.61	3.3	9.1	250	0.39	0.15	19.1	129

Notes. [a] Absolute FUV magnitude derived from the intrinsic rest-frame SED in mag.
[b] M_y, M_o, $M_\star$ are the masses of young, old stellar populations, and total stellar mass ($M_y + M_o$).
[c] $L(H\beta)$ is the $H\beta$ luminosity corrected for the Milky Way and internal extinction in erg s^{-1}.
[d] t_b is the starburst age in Myr.
[e] Star-formation rate corrected for the Milky Way and internal extinction, and escaping LyC radiation in M$_\odot$ yr^{-1}. [f] Specific star-formation rate in Gyr^{-1}.
[g] Exponential disc scale length in kpc.
[h] Galaxy radius, at which NUV intensity equal to half of maximal intensity in kpc.
[i] Star-formation rate surface density assuming galaxy radius equal to α in M$_\odot$ yr^{-1}kpc^{-2}.
[j] Star-formation rate surface density assuming galaxy radius equal to r_{50} in M$_\odot$ yr^{-1}kpc^{-2}.
[k] Acquisition image not obtained.
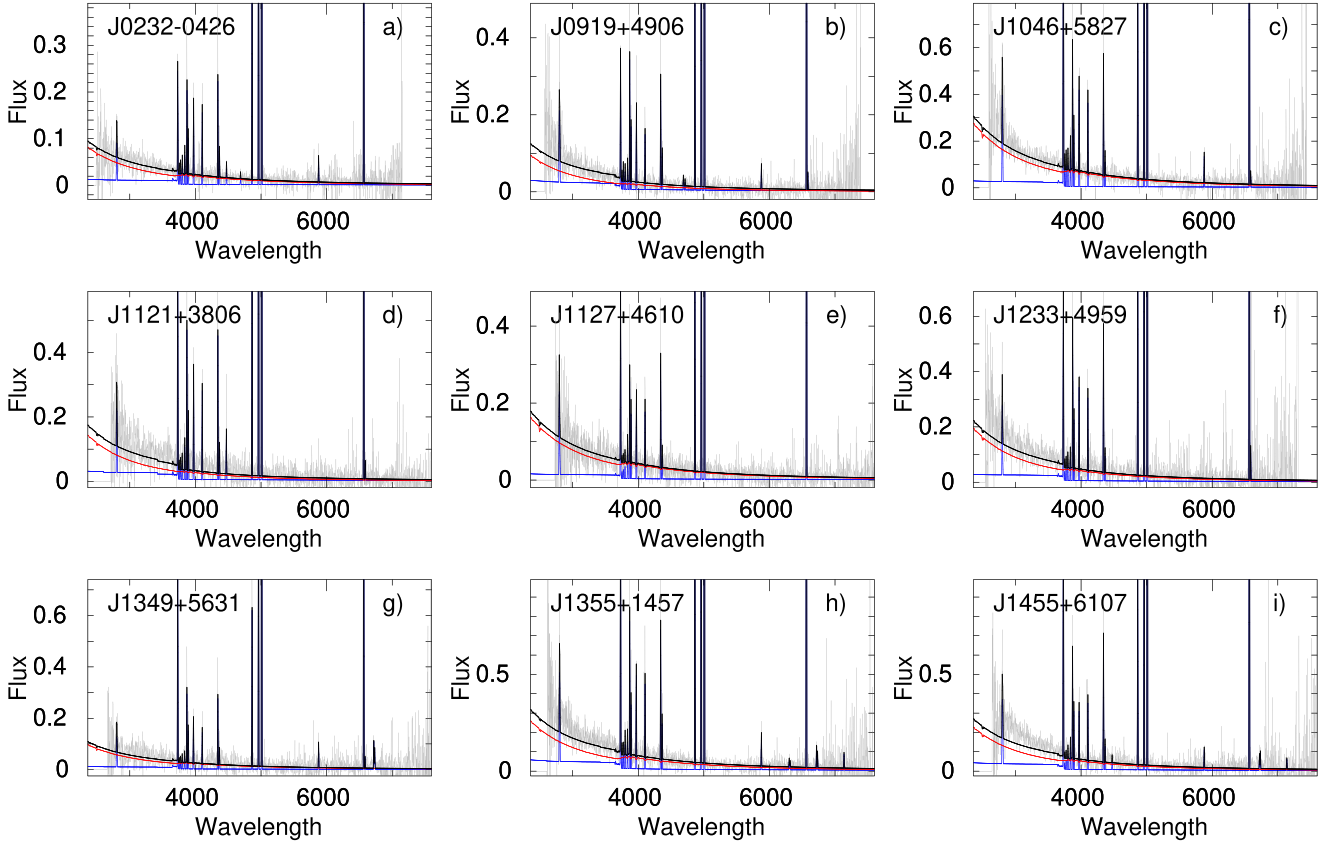
Figure 1. SED fitting of the galaxy SDSS spectra. The rest-frame spectra, corrected for Milky Way and internal extinction, are shown by grey lines. The total, nebular, and stellar modelled intrinsic SEDs are shown by black, blue, and red lines, respectively. Fluxes and wavelengths are expressed in 10^{-16} erg s^{-1} cm^{-2} Å^{-1} and Å, respectively.

galaxy (Fig. 2). Furthermore, the location of this galaxy inside the spectroscopic aperture is not known, introducing uncertainties in the fluxes of the COS spectra of J1046+5827. The only way to estimate these uncertainties is to compare the observed COS spectrum with the extrapolation of the SED, obtained from fitting the SDSS optical spectrum, to the UV range (see Section 5).

The spectra were obtained at COS Lifetime Position 4 with the low-resolution grating G140L and medium-resolution grating G160M, applying all four focal-plane offset positions. The 800 Å setup was used for the G140L grating (COS Lifetime Position 4: wavelength range 770–1950 Å, resolving power $R \simeq 1050$ at 1150 Å) to include the redshifted LyC emission for all targets.

Table 6. *HST*/COS observations.

Name	Date	Exposure time (s) (Central wavelength in Å)		
		MIRRORA	G140L	G160M
J0232−0426	2019-09-25	2 × 800	8211 (800)	3410 (1623)
J0919+4906	2020-04-30	2 × 900	8641 (800)	3499 (1611)
J1046+5827	2019-10-08	2 × 0[a]	7407[b] (800)	3910 (1600)
J1121+3806	2020-04-16	2 × 900	5551[b] (800)	3326 (1533)
J1127+4610	2020-01-10	2 × 900	8641 (800)	3497 (1533)
J1233+4959	2020-01-17	2 × 900	8641 (800)	3497 (1623)
J1349+5631	2020-03-12	2 × 800	8953 (800)	3916 (1577)
J1355+1457	2020-05-28	2 × 800	8232 (800)	3436 (1577)
J1455+6107	2020-03-09	2 × 900	9019 (800)	3760 (1577)

Notes. [a]Failed exposure.

[b]Partially executed observation.

We obtained resolved spectra of the galaxies' Ly α emission lines with the G160M grating ($R \sim 16\,000$ at 1600 Å), varying the G160M central wavelength with galaxy redshift to cover the emission line and the nearby continuum on a single detector segment. The G140L observations of J1046+5827 and J1121+3806 were partially executed due to technical problems (Table 6).

The individual exposures were reduced with the CALCOS pipeline v3.2.1, followed by accurate background subtraction and co-addition with custom software (Worseck et al. 2016). We used the same methods and extraction aperture sizes as in Izotov et al. (2018a,b) to achieve a homogeneous reduction of the galaxy sample observed in multiple programs. We checked the accuracy of our custom correction for scattered light in COS G140L data by comparing the LyC fluxes obtained in the total exposure and in orbital night, respectively. An exception is the galaxy J1046+5827, for which no orbital night exposures were obtained.

4 SURFACE BRIGHTNESS DISTRIBUTION IN THE NUV RANGE

The surface brightness (SB) profiles of our galaxies, in accord with previous studies by Izotov et al. (2016a,b, 2018a,b), are derived using the COS NUV acquisition images and the routine *ellipse* in IRAF[2]/STSDAS.[3] However, we note that the images of our galaxies are not as deep as those in Izotov et al. (2016a,b, 2018a,b) because of lower exposure times. The profiles were scaled to magnitudes per square arcsec using the ratios of the uncalibrated galaxy fluxes in the COS NUV images, measured with the routine *apphot* in IRAF, to the fluxes corresponding to the respective apparent *GALEX* NUV magnitudes. An exception is the galaxy J1121+3806, for which no *GALEX* data are available. For this galaxy, we adopt a magnitude

[2]IRAF is distributed by the National Optical Astronomy Observatories, which are operated by the Association of Universities for Research in Astronomy, Inc., under cooperative agreement with the National Science Foundation.
[3]STSDAS is a product of the Space Telescope Science Institute, which is operated by AURA for NASA.

derived from extrapolation of the attenuated SED obtained from the SDSS spectrum. There is no SB profile for the galaxy J1046+5827 because its acquisition exposure failed, as noted before.

As found before by Izotov et al. (2016a,b, 2018a,b), the outer parts of our galaxies are characterized by a linear decrease in SB (in mag per square arcsec scale), characteristic of a disc structure, while the central part with the bright star-forming region(s) shows a sharp increase (Fig. 3).

The scale lengths α of our galaxies, defined in equation (1) of Izotov et al. (2016b), are in the range ~ 0.3–0.6 kpc (Fig. 3), lower than $\alpha = 0.6$–1.8 kpc in other LyC leakers (Izotov et al. 2016a,b, 2018a,b) and indicating a lower mass and a more compact structure for our galaxies. The corresponding surface densities of star-formation rate in the studied galaxies $\Sigma = \text{SFR}/(\pi \alpha^2)$ are similar to those of other LyC leakers. Because the bright star-forming regions are very compact with sharply rising brightness profiles, the half-light radii r_{50} of our galaxies in the NUV are similar but considerably smaller than α (see Table 5). Adopting r_{50} as a measure of the size of these galaxies, the corresponding Σs are typically two orders of magnitude larger, and are comparable to those found for SFGs at high redshifts (Curtis-Lake et al. 2016; Bouwens et al. 2017; Paulino-Afonso et al. 2018). The values Σ_1 in Table 5 are similar to those found by Kim et al. (2020) for GPs and Lyman Break Analogues.

5 COMPARISON OF THE *HST*/COS SPECTRA WITH THE MODELLED SEDS IN THE UV RANGE

To derive the fraction of the escaping ionizing radiation, the two methods, which we use (e.g. Izotov et al. 2018a), are based on the comparison between the observed flux in the Lyman continuum range and the intrinsic flux produced by stellar populations in the galaxy. The intrinsic LyC flux can be obtained from SED fitting of the SDSS spectra or from the flux of the H β emission line. To verify the quality of our SED fitting, we extrapolate the attenuated SEDs to the UV range and compare them with the observed COS spectra in Fig. 4. For comparison, we also show with blue filled circles the *GALEX* FUV and NUV fluxes and the fluxes in the SDSS u, g, r, i, z filters. We find that the spectroscopic and photometric data in the optical range are consistent, indicating that almost all the emission of our galaxies is inside the spectroscopic aperture. Therefore, aperture corrections are not needed. On the other hand, considerable deviations of *GALEX* FUV and NUV fluxes to brighter values from both the observed COS spectra and attenuated SED extrapolations are found for many of galaxies, most strikingly for J0232−0426. These deviations in the FUV could in part be explained by the redshifted Ly α. However, no such deviation is seen in the spectrum of J0919+4906 with the highest EW(Ly α). Furthermore, no bright emission lines fall into the NUV range despite large deviations from the observed spectra and modelled SEDs. Therefore, these systematic deviations indicate high uncertainties of the *GALEX* FUV and NUV fluxes, at least for faint objects.

The modelled intrinsic SEDs in Fig. 4 are attenuated by adopting the extinction coefficients $C(\text{H}\beta)_{\text{MW}}$ and $C(\text{H}\beta)_{\text{int}}$ (Table 3) and the reddening law by Cardelli et al. (1989) with $R(V)_{\text{MW}} = 3.1$ and $R(V)_{\text{int}} = 2.7$ (black solid lines and red solid lines, respectively).

It is seen in Fig. 4 that the models reproduce the SDSS spectra quite well and do not depend on the adopted $R(V)_{\text{int}}$ because of low extinction. There is a stronger dependence of the attenuated SEDs on $R(V)_{\text{int}}$ in the UV range, but differences of the attenuated SEDs with $R(V)_{\text{int}} = 3.1$ and $R(V)_{\text{int}} = 2.7$ are still small (black and red lines in Fig. 4), because of small extinction coefficients
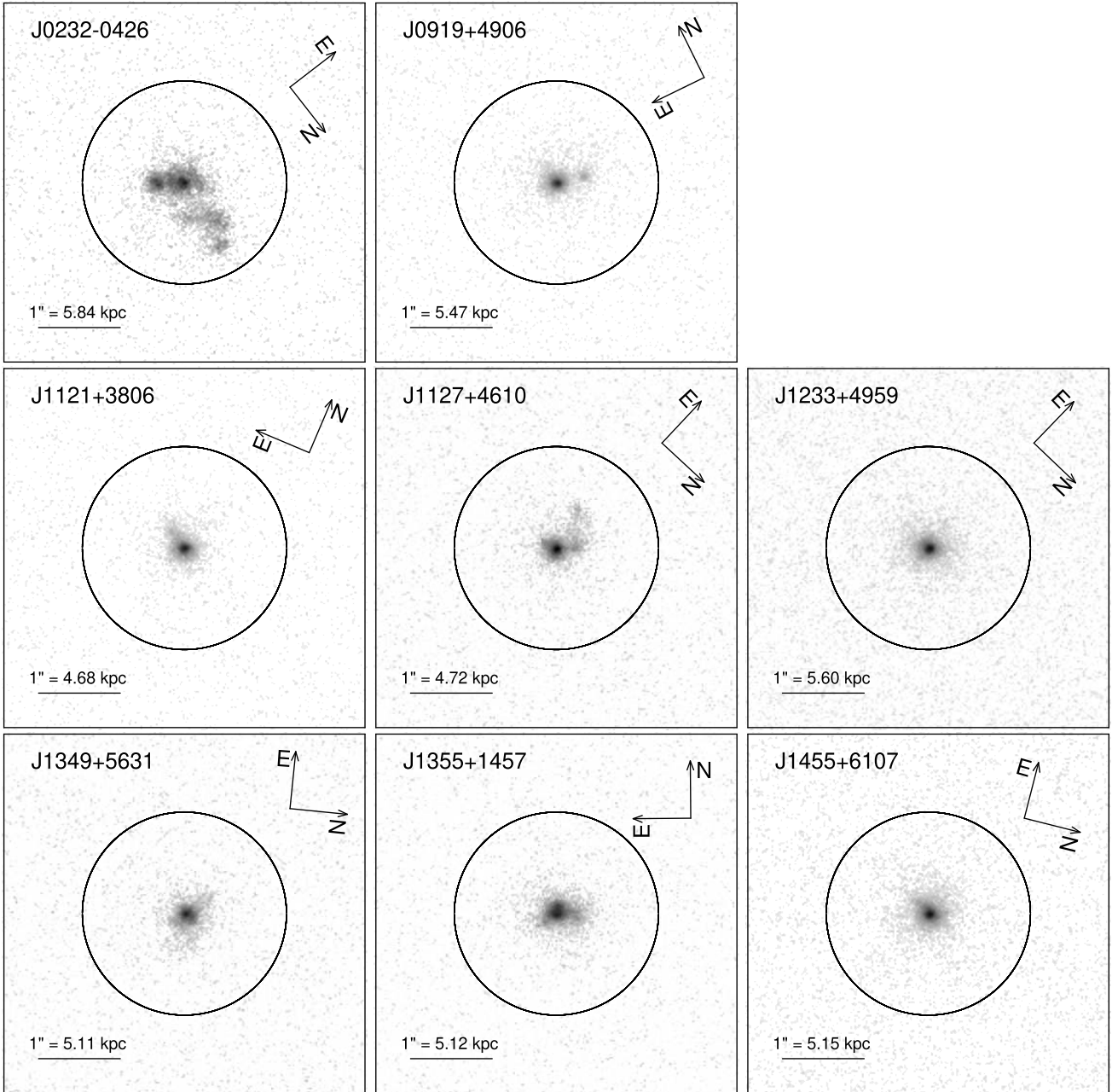
Figure 2. The *HST* NUV acquisition images of the candidate LyC leaking galaxies in a log surface brightness scale. The COS spectroscopic aperture with a diameter of 2.5 arcsec is shown in all panels by a circle. The linear scale in each panel is derived adopting an angular size distance.

$C(H\beta)_{int}$. However, the attenuated SEDs with $R(V)_{int} = 2.7$ reproduce on average somewhat better the observed COS spectra.

6 LY α EMISSION

A resolved Lyα λ1216 Å emission line is detected in the medium-resolution spectra of all galaxies (Fig. 5), whereas this line is unresolved in the low-resolution spectra. The shape of the resolved Ly α line is similar to that observed in most known LyC leakers (Izotov et al. 2016a,b, 2018a,b) and in some other galaxies (Jaskot & Oey 2014; Henry et al. 2015; Yang et al. 2017a; Izotov et al. 2020). In the present sample, profiles with two peaks are detected in the spectra of seven galaxies. The signal-to-noise ratio in the spectrum

of J0232−0426 is too low to definitely derive the profile of its Ly α emission line. The Ly α profile of J1127+4610 may show more than two peaks, but the S/N ∼ 5 even in undersampled spectra is too low to definitely determine that, similar to the data of J0232−0426. The parameters of Ly α emission are shown in Table 7.

We show in Fig. 6 the dependence of some Ly α characteristics on absolute FUV magnitude. Our galaxies with detected LyC emission are shown by red filled circles and those with upper limits of LyC emission are represented by red open circles. All our low-mass galaxies are characterized by moderate Ly α luminosities in a narrow range between $10^{42.19}$ and $10^{42.74}$ erg s^{-1} (Fig. 6a), that are slightly below the values for confirmed LyC leakers (blue filled circles) by Izotov et al. (2016a,b, 2018a,b) and high-redshift galaxies (grey
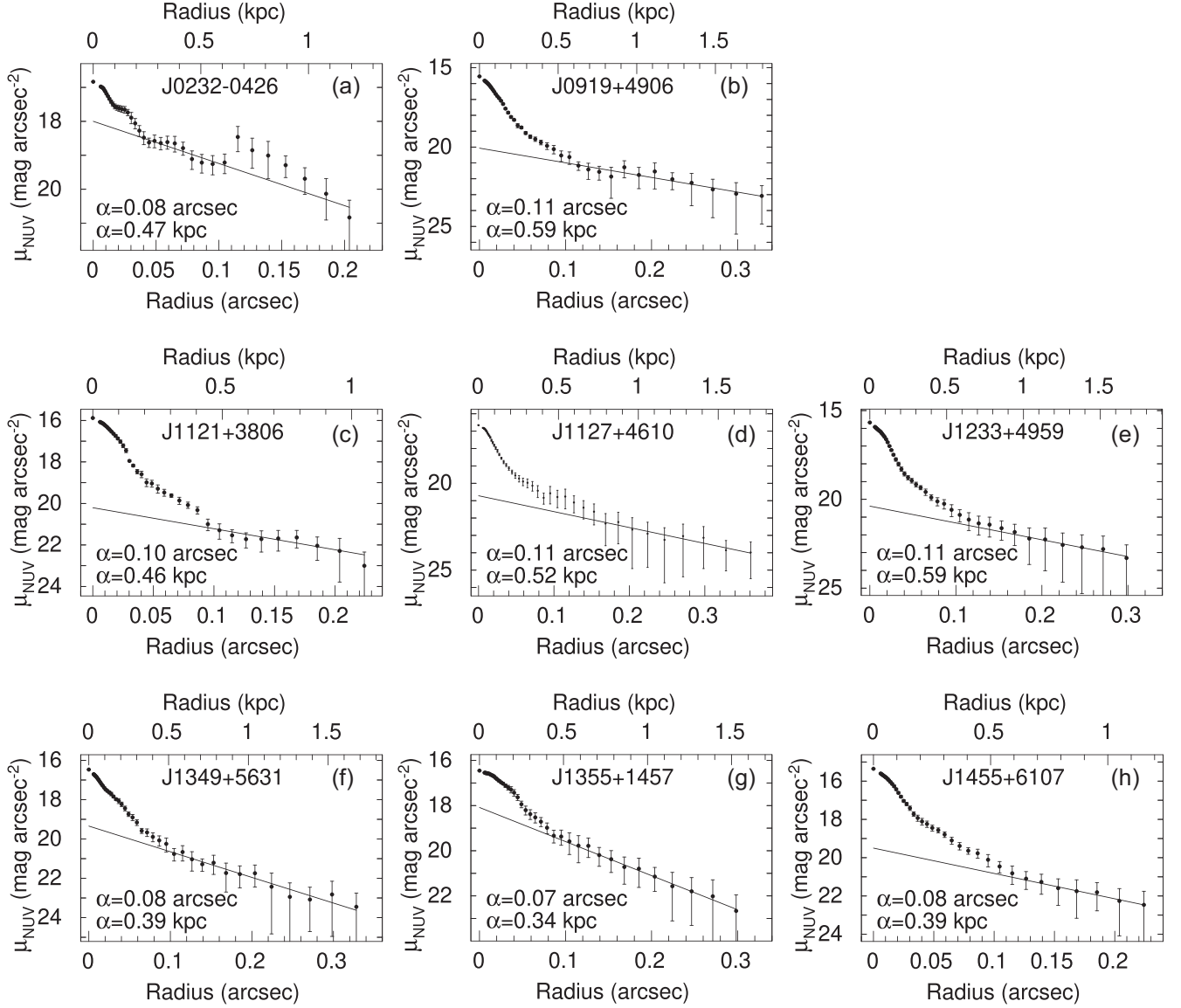
Figure 3. NUV surface brightness profiles of galaxies.

open circles) by Ouchi et al. (2008), Hashimoto et al. (2017), Jiang et al. (2018), Matthee et al. (2017), Matthee et al. (2018), Sobral et al. (2018), but are ∼1 order of magnitude higher than those for GPs (black asterisks; Jaskot & Oey 2014; Henry et al. 2015; Jaskot et al. 2017; Yang et al. 2017a; McKinney et al. 2019). Our low-mass galaxies have high EW(Ly α) ∼ 65–220 Å (Table 7, red symbols in Fig. 6b), similar to those in other LyC leakers (blue symbols in Fig. 6b). They are at the high end of the EW(Ly α) values for high-z LAEs by Ouchi et al. (2008), Hashimoto et al. (2017), Jiang et al. (2018), Harikane et al. (2018), Caruana et al. (2018), Pentericci et al. (2018), Matthee et al. (2017, 2018), Sobral et al. (2018) (grey open circles) and GPs (black asterisks). However, contrary to expectations for galaxies with lower stellar masses and, likely, lower masses of the neutral gas, the separation between the Ly α peaks is on average similar to that in higher mass LyC leakers (Fig. 6c), and it is higher in galaxies with upper limits of LyC emission (>400 km s^{-1}, red open circles). Ly α escape fractions f_{esc}(Ly α) in low-mass galaxies are also similar to those in higher mass LyC leakers, and they are lower in galaxies with upper limits of LyC emission (red open circles

in Fig. 6d). We also note that the average ratio of blue and red peak fluxes of ∼25 per cent (Table 7) is somewhat lower than the value of ∼30 per cent quoted by Hayes et al. (2021) for z ∼ 0 galaxies.

For comparison, we also show by green filled circles in Fig. 6 the extreme-O_{32} low-redshift (z < 0.07) compact SFGs with high EW(Ly α) and by green open circles the galaxies with weak Ly α emission on top of broad Ly α absorption profiles. It is seen that low-z SFGs with high EW(Ly α) are shifted from relations for high-z LAEs (black solid lines) to lower L(Ly α) (Fig. 6a) and EW(Ly α) (Fig. 6b), despite similar excitation conditions, as indicated by comparable O_{32} and EW(H β) values.

Izotov et al. (2020) discussed this feature of low-z CSFGs and suggested that it could be due to the presence of an extended Ly α halo with an angular diameter considerably larger than the 2.5 arcsec in diameter COS spectroscopic aperture, making some Ly α emission unobservable, although there is no direct evidence for that from the *HST* observations. Furthermore, the Ly α escape fraction f_{esc}(Ly α) in these galaxies is somewhat lower than that in LyC leakers (Figs 6d), supporting the idea of the extended Ly α halo, exceeding the size of
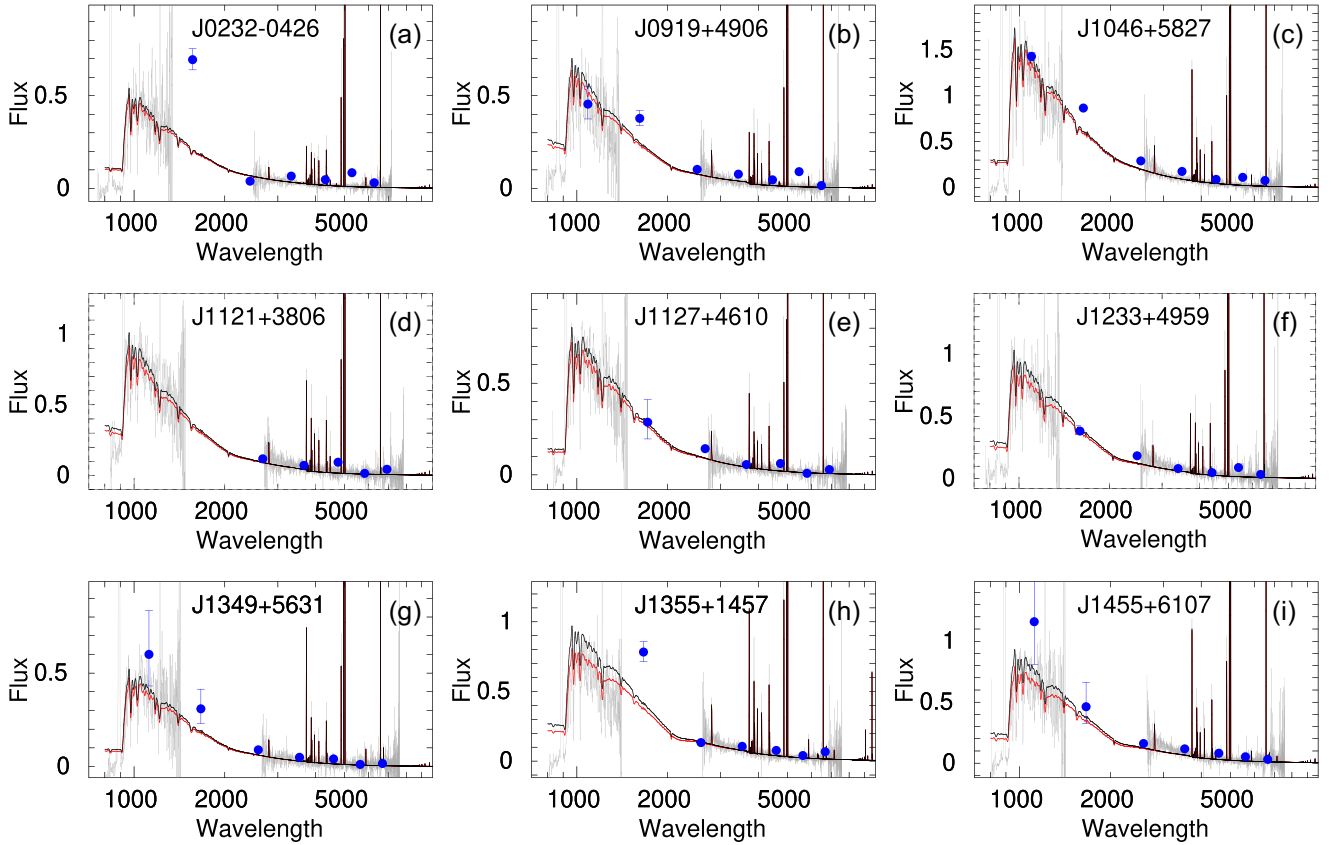
Figure 4. A comparison of the COS G140L and SDSS spectra (grey lines), and photometric data (blue filled circles) with the modelled SEDs. *GALEX* FUV and NUV fluxes with 1σ error bars and SDSS fluxes in u, g, r, i, z bands are shown by blue-filled circles. Modelled intrinsic SEDs, which are reddened by the Milky Way extinction with $R(V)_{\rm MW} = 3.1$ and internal extinction with $R(V)_{\rm int} = 3.1$ and 2.7, are shown by black and red solid lines, respectively. Fluxes are in 10^{-16} erg s^{-1} cm^{-2}Å^{-1}, wavelengths are in Å.

the COS spectroscopic aperture, corresponding to a linear radius of ~ 0.6–1.7 kpc at the redshifts of low-z CSFGs. This results in a loss of some emission and, consequently, in a reduced derived value of $f_{\rm esc}({\rm Ly}\,\alpha)$. However, the linear radius inside the COS spectroscopic aperture at redshift $z > 0.3$ is $\gtrsim 5$ kpc and, likely, is larger than the extent of Ly α emission, implying that most of Ly α emission is inside the COS aperture, despite the fact that the luminosity of Ly α in LyC leakers (red and blue circles in Fig. 6) is several times higher than that in low-z CSFGs with extreme O$_{32}$.

7 ESCAPING LYMAN CONTINUUM RADIATION

The observed G140L total-exposure spectra with the LyC spectral region (grey lines) and predicted intrinsic SEDs (blue dash-dotted lines) are shown in Fig. 7, together with the attenuated intrinsic SEDs (red solid lines). The predicted intrinsic SEDs are obtained from fitting the optical SDSS spectra, corrected for the Milky Way extinction at observed wavelengths, and adopting $A(V)_{\rm MW}$ from the NED, and for the internal extinction at rest-frame wavelengths, the UV attenuation law with $R(V) = 2.7$, and the extinction coefficients $C({\rm H}\,\beta)_{\rm int}$ derived from the hydrogen Balmer decrement.

The level of the observed LyC continuum is indicated by horizontal red lines shortwards of the vertical dotted line showing the Lyman series limit. The Lyman continuum emission is detected in the spectra of four galaxies, J0919+4906, J1121+3806, J1127+4610, and J1233+4959 and only upper limits are derived

in the spectra of the remaining galaxies. The measurements are summarized in Table 8. Due to the faintness of the targets, we adopted the LyC fluxes measured during orbital night (except for J1046+5827) to minimize residual uncertainties in the scattered light correction.

Izotov et al. (2016a,b, 2018a,b) used the ratio of the escaping fluxes $I_{\rm esc}$ to the intrinsic fluxes $I_{\rm mod}$ of the Lyman continuum to derive $f_{\rm esc}({\rm LyC})$:

$$f_{\rm esc}({\rm LyC}) = \frac{I_{\rm esc}(\lambda)}{I_{\rm mod}(\lambda)}, \qquad (1)$$

where λ is the mean wavelength of the range used for averaging of the LyC flux density (see Table 8). Izotov et al. (2016b) proposed two methods to derive iteratively the intrinsic fluxes $I_{\rm mod}$ and, correspondingly, the LyC escape fractions $f_{\rm esc}({\rm LyC})$: (1) from the SED fitting and (2) from the equivalent width of the H β emission line and its extinction-corrected flux and adopting relations between $I({\rm H}\,\beta)/I_{\rm mod}$ and EW(H β) from the models of photoionized H II regions (equation 4 for instantaneous burst in Izotov et al. 2016b). We use both methods in this paper.

The escape fraction $f_{\rm esc}({\rm LyC})$, in the range between 11 and 35 per cent, is derived in four out of nine galaxies (Table 8). For the remaining galaxies, only upper limits of $f_{\rm esc}({\rm LyC})$ were derived. We note that the $f_{\rm esc}({\rm LyC})$s derived by the second method are somewhat lower than those derived by the first method, but are consistent within the errors for most galaxies.
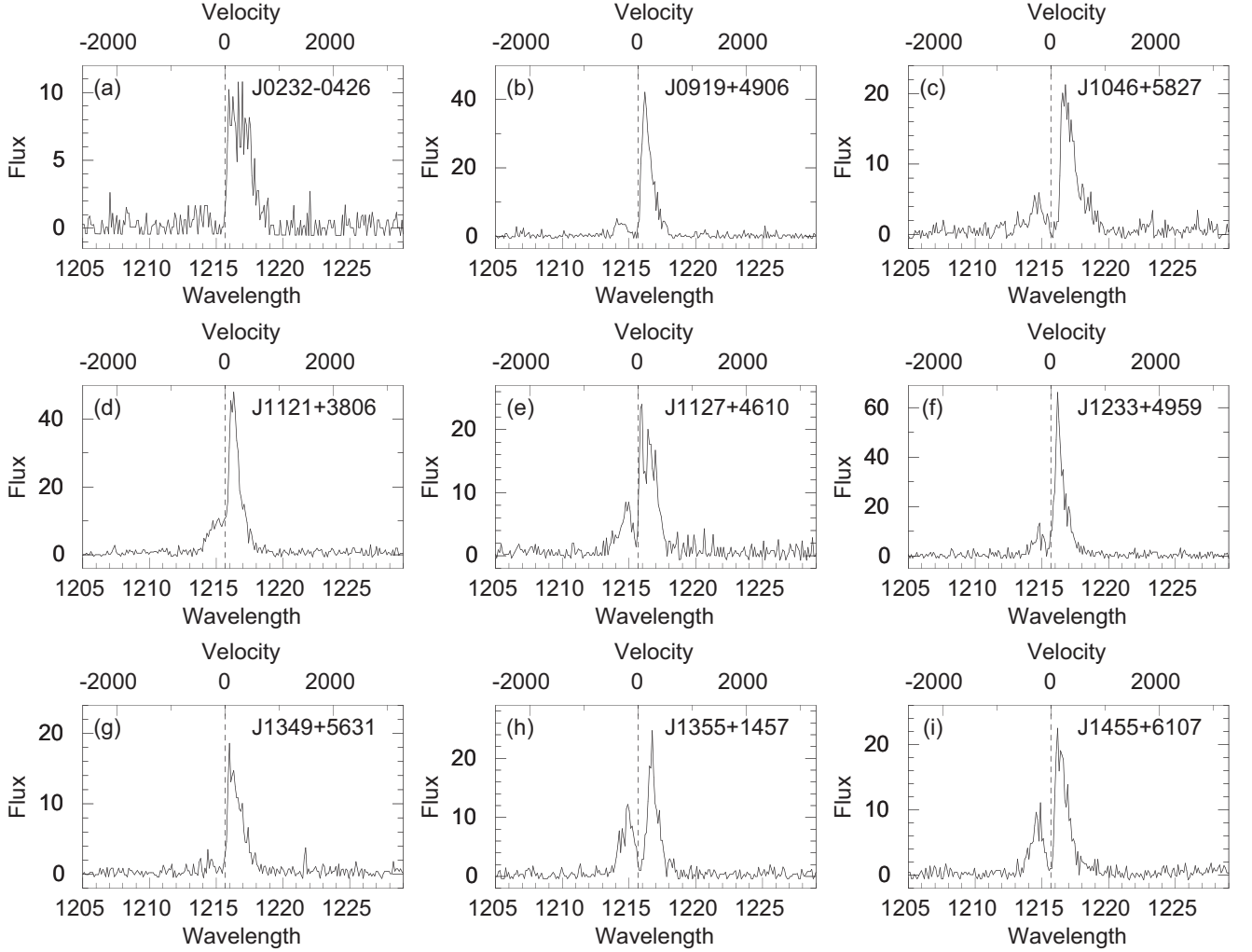
Figure 5. Ly α profiles. The vertical dashed lines indicate the rest-frame wavelength of 1215.67 Å for Ly α. Fluxes are in 10^{-16} erg s^{-1} cm^{-2}Å^{-1}, rest-frame wavelengths are in Å and velocities are in km s^{-1}.

Table 7. Parameters for the Ly α emission line.

Name	$A(Ly\alpha)_{MW}$ [a]	I [b]	$\log L$ [c]	EW[d]	V_{sep} [e]	Blue/red[f]	$f_{esc}(Ly\alpha)$ [g]
J0232−0426	0.106	43.5 ± 6.4	42.53	90.6 ± 1.8	446.0 ± 51.8	9.8	42.5 ± 5.3
J0919+4906	0.110	81.7 ± 9.5	42.68	219.5 ± 3.7	369.2 ± 44.9	11.6	68.7 ± 8.9
J1046+5827	0.059	65.3 ± 8.2	42.57	65.3 ± 2.2	512.6 ± 58.7	19.0	31.8 ± 4.3
J1121+3806	0.154	79.5 ± 8.6	42.43	142.3 ± 2.9	229.3 ± 79.5	23.1	43.2 ± 5.2
J1127+4610	0.123	44.4 ± 5.6	42.18	94.3 ± 2.2	259.4 ± 51.8	28.8	39.7 ± 8.5
J1233+4959	0.124	83.6 ± 9.7	42.74	152.0 ± 6.7	271.9 ± 27.6	16.9	41.2 ± 3.9
J1349+5631	0.070	47.0 ± 5.6	42.33	95.1 ± 3.2	386.5 ± 56.3	9.1	40.3 ± 4.4
J1355+1457	0.152	68.9 ± 7.3	42.50	151.6 ± 2.9	430.4 ± 69.1	63.3	23.1 ± 2.8
J1455+6107	0.098	74.0 ± 8.4	42.54	144.0 ± 2.7	388.9 ± 41.5	41.5	36.5 ± 4.5

Notes. [a]Milky Way extinction at the observed wavelength of the Ly α emission line in mags adopting Cardelli et al. (1989) reddening law with $R(V) = 3.1$.
[b]Flux in 10^{-16} erg s^{-1} cm^{-2} measured in the COS spectrum and corrected for the Milky Way extinction.
[c] L is Ly α luminosity in erg s^{-1} corrected for the Milky Way extinction.
[d]Rest-frame equivalent width in Å.
[e]Ly α peak separation in km s^{-1}.
[f]Flux ratio of blue-to-red peaks in per cent.
[g]Ly α escape fraction in per cent.
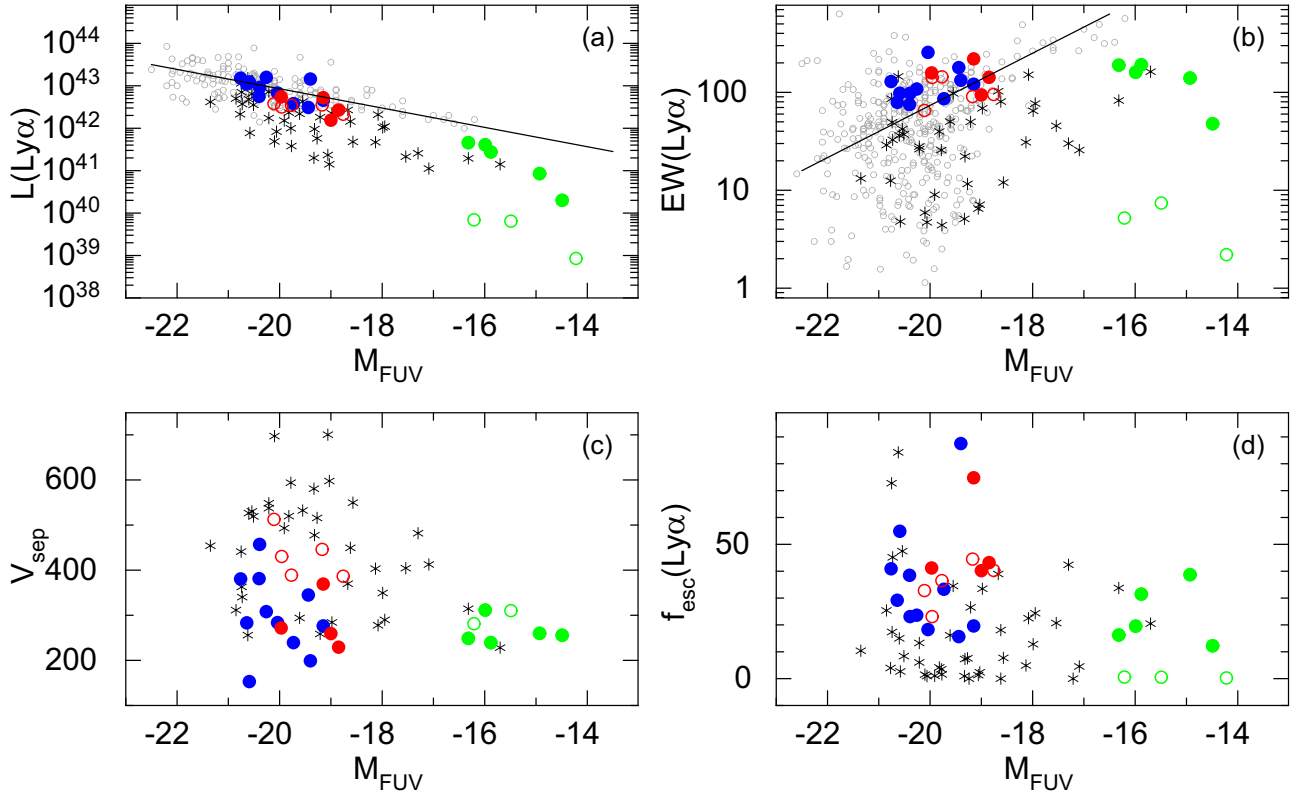
Figure 6. Dependence of absolute magnitude $M_{\rm FUV}$ at 1500 Å in mags on (a) Ly α luminosity $L({\rm Ly}\,\alpha)$ in erg s^{-1}, (b) equivalent width EW(Ly α) in Å, (c) separation between Ly α peaks in km s^{-1}, and (d) Ly α escape fraction $f_{\rm esc}({\rm Ly}\,\alpha)$ in per cent. Galaxies from this paper with detected LyC emission and with upper limits of LyC emission are shown by red filled and open circles, respectively. The confirmed LyC leakers from Izotov et al. (2016a,b, 2018a,b) are shown by blue filled circles. GPs (Jaskot & Oey 2014; Henry et al. 2015; Jaskot et al. 2017; Yang et al. 2017a; McKinney et al. 2019) are shown by black asterisks. High-redshift galaxies from Ouchi et al. (2008), Hashimoto et al. (2017), Jiang et al. (2018), Matthee et al. (2017, 2018), Sobral et al. (2018) in (a) and from Ouchi et al. (2008), Hashimoto et al. (2017), Jiang et al. (2018), Harikane et al. (2018), Caruana et al. (2018), Pentericci et al. (2018), Matthee et al. (2017, 2018), Sobral et al. (2018) in (b) are represented by small grey open circles. Relations for these galaxies are shown by black solid lines. For comparison, the green symbols show $z < 0.07$ compact SFGs with extreme $O_{32} > 20$ (Izotov et al. 2020), where filled symbols are for galaxies with high EW(Ly α) without evidence of the Ly α absorption profiles, whereas open symbols are for galaxies with low-EW Ly α emission on the top of broad absorption.

8 INDICATORS OF HIGH LYC ESCAPE FRACTION

The direct detection of LyC emission in low-redshift SFGs is a difficult task. At the moment, only *HST* can be used for that purpose. Therefore, reasonable indirect indicators of LyC leakage at low redshift are needed to build a larger sample for statistical studies.

Jaskot & Oey (2013) and Nakajima & Ouchi (2014) proposed a high O_{32} ratio as an indication of escaping ionizing radiation. We have in hand, with our new LyC leakers, a sample of twenty five galaxies with a wide range of $O_{32} \sim 0.5$–27 and directly derived $f_{\rm esc}({\rm LyC})$ (Leitet et al. 2013; Borthakur et al. 2014; Leitherer et al. 2016; Izotov et al. 2016a, b, 2018a, b). The $f_{\rm esc}({\rm LyC})$ values for several LyC leakers from Leitet et al. (2013) and Leitherer et al. (2016) are discrepant. Therefore, for these galaxies, we have used the $f_{\rm esc}({\rm LyC})$ values re-analysed by Chisholm et al. (2017). The relation between $f_{\rm esc}({\rm LyC})$ and O_{32} is presented in Fig. 8(a). It has been discussed before by Faisst (2016) and Izotov et al. (2018b). There is a trend of increasing $f_{\rm esc}({\rm LyC})$ with increasing of O_{32}, but with a substantial scatter, at large O_{32} values. The large scatter is due to the dependence of O_{32} on other parameters such as metallicity, hardness of ionizing radiation and ionization parameter. Additionally, the spread of $f_{\rm esc}({\rm LyC})$ can also be caused by inhomogeneous leakage through channels with low optical depth and their orientation relative to

the observer. Therefore, a high O_{32} is not a very certain indicator of high $f_{\rm esc}({\rm LyC})$ and it is only a necessary condition for escaping radiation (Izotov et al. 2018b; Nakajima et al. 2020). The only definite result from Fig. 8(a) is that $f_{\rm esc}({\rm LyC})$ is very low in objects with $O_{32} \leq 4$.

It has also been suggested that $f_{\rm esc}({\rm LyC})$ tends to be higher in low-mass galaxies (Wise et al. 2014; Trebitsch et al. 2017). Our new nine galaxies with $M_\star < 10^8\,{\rm M}_\odot$ considerably extend the mass range down to a stellar mass of $\sim 10^7\,{\rm M}_\odot$, similar to the lowest mass known of high-z leakers (Vanzella et al. 2020). Previous observations have shown a slight tendency for $f_{\rm esc}({\rm LyC})$ to increase with decreasing stellar mass, albeit with a large intrinsic scatter. We present in Fig. 8(b) the relation between $f_{\rm esc}({\rm LyC})$ and stellar mass $M_\star$, including our new data. The added data shows, on the contrary, that there is no clear correlation between $f_{\rm esc}({\rm LyC})$ and $M_\star$. This is one of the important findings of this study: contrary to expectation, there is no clear trend of increasing $f_{\rm esc}({\rm LyC})$ with decreasing $M_\star$. However, we caution that $M_\star$ might be higher than those derived from SED fitting because of uncertainties in the determination of the mass of the old stellar population.

In Fig. 8(c), we show the relation $f_{\rm esc}({\rm LyC}) - f_{\rm esc}({\rm Ly}\,\alpha)$ for the $z \lesssim 0.45$ LyC leakers observed by Izotov et al. (2016a,b, 2018a,b). There is a tendency for $f_{\rm esc}({\rm LyC})$ to increase with increasing $f_{\rm esc}({\rm Ly}\,\alpha)$. However, the spread of the data is large. The only
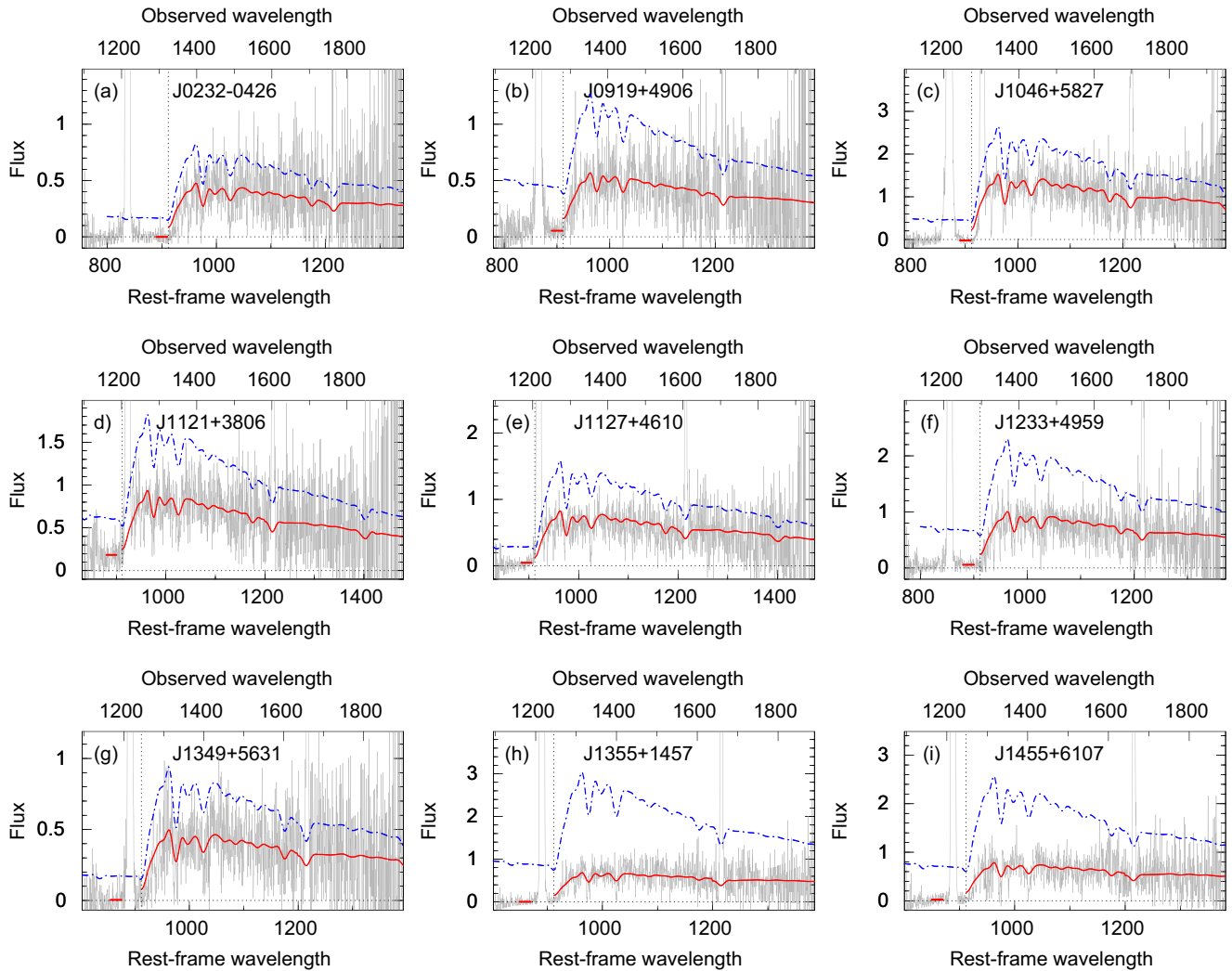
Figure 7. COS G140L spectra of our sources (grey lines) superposed by the modelled SEDs (thick red solid lines), reddened by both the internal and Milky Way extinctions. The unreddened (intrinsic) SEDs are shown by the thick blue dash-dotted lines. $R(V)_{\rm int} = 2.7$ is adopted in all panels. The Lyman limit at the rest-frame wavelength 912 Å is indicated by dotted vertical lines. Zero flux is represented by dotted horizontal lines. Fluxes are in $10^{-16}\,{\rm erg\,s^{-1}\,cm^{-2}\,\AA^{-1}}$, wavelengths are in Å.

important results are: (1) $f_{\rm esc}({\rm LyC}) < f_{\rm esc}({\rm Ly\,\alpha})$ for the majority of galaxies, in agreement with theoretical predictions (Dijkstra, Gronke & Venkatesan 2016) and (2) $f_{\rm esc}({\rm LyC})$ is very low for $f_{\rm esc}({\rm Ly\,\alpha}) \lesssim 20$ per cent.

The profile of the Ly α emission line can also be used as an indirect indicator of the LyC leakage. This indicator is most useful because it can be applied to nearby low-mass galaxies, for which direct observations of the LyC with *HST*/COS are not possible because of their low redshift. Verhamme et al. (2017) and Izotov et al. (2018b) found a tight dependence of $f_{\rm esc}({\rm LyC})$ on the separation $V_{\rm sep}$ between the peaks of the Ly α emission line in LyC leakers. The new low-mass LyC leakers discussed in this paper also follow the relation discussed by Izotov et al. (2018b), shown by the solid line in Fig. 8(d). There is no new galaxy having a peak separation less than $230\,{\rm km\,s^{-1}}$. For comparison, the lowest peak separation in the sample of low-z leakers (Izotov et al. 2018b), is that of J1243+4646, $\sim150\,{\rm km\,s^{-1}}$. We note that Meyer et al. (2021) have recently reported the discovery of a double-peak Ly α profile in the galaxy A370p_z1, at the epoch of reionization ($z = 6.803$), with the extremely low peak separation of $110\,{\rm km\,s^{-1}}$, implying an extremely high LyC escape fraction.

The relation between $V_{\rm sep}$ and $f_{\rm esc}({\rm LyC})$, as shown in Fig. 8(d), is a consequence of the fractions of LyC and Ly α escaping radiation being determined by the column density of the neutral gas along the line of sight in LyC leaking galaxies (e.g. Verhamme et al. 2015, 2017). The majority of the new observations of low-mass galaxies (red symbols) support previous findings. However, there is one galaxy, J0919+4906, which deviates significantly from the relation of Izotov et al. (2018b). It has a $f_{\rm esc}({\rm LyC})$ corresponding to $V_{\rm sep}$ of $\sim250\,{\rm km\,s^{-1}}$ derived from the relation, compared to the measured value of $\sim370\,{\rm km\,s^{-1}}$. The cause of this deviation is not clear.

This relation should constitute a strong constraint for constructing radiative transfer and kinematical models which simultaneously reproduce $f_{\rm esc}({\rm LyC})$ and the Ly α profile.

Izotov et al. (2018b) considered also another potential indicator of escaping LyC radiation. They found that the stellar line O VI λ1035 Å with a P-Cygni profile is seen in the spectra of most LyC leaking galaxies observed by Izotov et al. (2016a,b, 2018a,b), indicative of hot most massive stars with masses of $\sim100\,{\rm M}_\odot$. It is likely that stellar winds from these hot stars produce channels

Table 8. LyC escape fraction.

Name	$\lesssim mbda_0$ [a] (Å)	$A(LyC)_{MW}$ [b] (mag)	I_{mod} [c,d]	$I_{obs}(total)$ [c,e]	$I_{esc}(total)$ [c,f]	f_{esc} [g] (per cent)	f_{esc} [h] (per cent)
J0232−0426	870-890	0.203	16.83 ± 1.92	$<0.58^{i}$	<0.70	<4.2	<1.6
J0919+4906	890-910	0.144	44.35 ± 3.70	$6.30^{+1.67}_{-1.51}$	$7.19^{+1.92}_{-1.73}$	$16.2^{+5.9}_{-5.3}$	$15.1^{+4.5}_{-4.2}$
J1046+5827	890-910	0.080	46.65 ± 4.87	$<0.80^{i}$	<0.86	<1.8	<1.0
J1121+3806	880-900	0.210	60.69 ± 5.30	$17.53^{+2.16}_{-2.09}$	$21.25^{+2.61}_{-2.52}$	$35.0^{+5.6}_{-5.4}$	$25.1^{+3.8}_{-3.7}$
J1127+4610	870-900	0.165	29.00 ± 3.02	$2.76^{+0.89}_{-0.83}$	$3.22^{+1.06}_{-0.99}$	$11.1^{+4.0}_{-3.7}$	$6.1^{+2.4}_{-2.3}$
J1233+4959	890-910	0.158	66.81 ± 6.51	$7.00^{+1.69}_{-1.61}$	$8.09^{+1.95}_{-1.86}$	$12.1^{+3.4}_{-3.3}$	$9.5^{+2.9}_{-2.7}$
J1349+5631	850-870	0.098	17.22 ± 1.87	$<1.05^{i}$	<1.15	<6.7	<2.2
J1355+1457	850-870	0.208	86.01 ± 8.77	$<0.85^{i}$	<1.03	<1.2	<0.9
J1455+6107	850-870	0.133	69.42 ± 6.97	$<1.36^{i}$	<1.54	<2.2	<1.9

Notes. [a]Rest-frame wavelength range in Å used to determine the LyC flux.
[b]Milky Way extinction at the mean observed wavelengths of the range used to determine the LyC flux. The Cardelli et al. (1989) reddening law with $R(V) = 3.1$ is adopted.
[c]LyC flux in 10^{-18} erg s^{-1} cm^{-2} Å^{-1}.
[d]LyC flux derived from the modelled SED.
[e]Observed LyC flux derived from the spectrum with shadow exposure, excluding J1046+5827, where measurements are from the spectrum with total exposure.
[f]LyC flux which is corrected for the Milky Way extinction.
[g] $f_{esc}(LyC) = I_{esc}(total)/I_{mod}$, where I_{mod} is derived from SED (first method).
[h] $f_{esc}(LyC) = I_{esc}(total)/I_{mod}$, where I_{mod} is derived from H β flux (second method).
[i]1σ confidence upper limit.
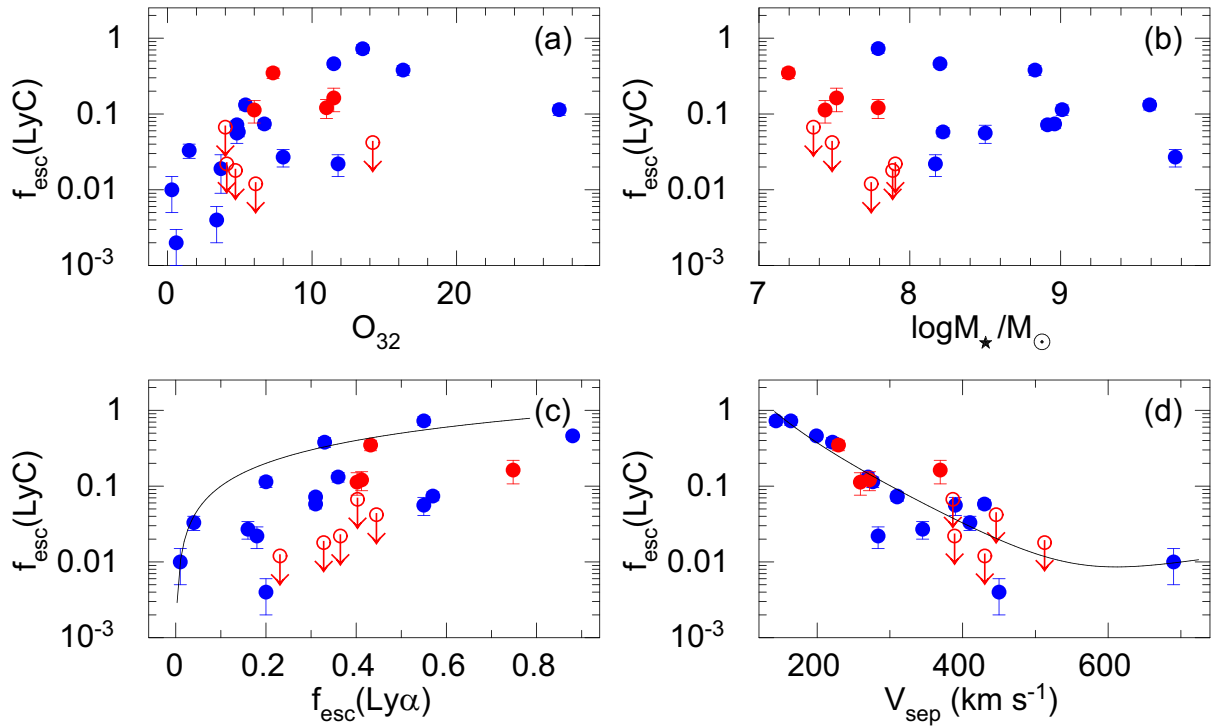
Figure 8. Relations between the Lyman continuum escape fraction $f_{esc}(LyC)$ in low-redshift LyC leaking galaxies derived from the SED fits and (a) the [O III]λ5007/[O II]λ3727 emission-line flux ratio, (b) the stellar mass $M_\star$, (c) the Ly α escape fraction $f_{esc}(Ly \alpha)$, and (d) the separation V_{sep} between the Ly α profile peaks. LyC leakers from Izotov et al. (2016a,b, 2018a,b), Leitet et al. (2013), Borthakur et al. (2014), and Leitherer et al. (2016) are shown by blue filled circles with 1σ errors, the galaxies from this paper with detected LyC emission and upper limits are represented by red filled circles with 1σ errors and red open circles and downward arrows, respectively. The solid line in (c) is the equality line and the solid line in (d) represents the relation from Izotov et al. (2018b).

with ionized gas, through which ionizing radiation escapes the galaxy.

In Fig. 9, we present segments of COS G140L spectra of the LyC leakers studied in this paper, in the wavelength range ~1000–1300 Å, which includes the stellar lines O VI λ1035 Å

and N V λ1240 Å. At variance with the results of Izotov et al. (2016a,b, 2018a,b), the O VI λ1035 Å lines are not seen in spectra of our galaxies, including the galaxy J1121+3806 with the highest $f_{esc}(LyC) = 35.0$ per cent. Hints of this line are likely seen in the spectra of J1046+5827, J1349+5632, and J1233+4959 with

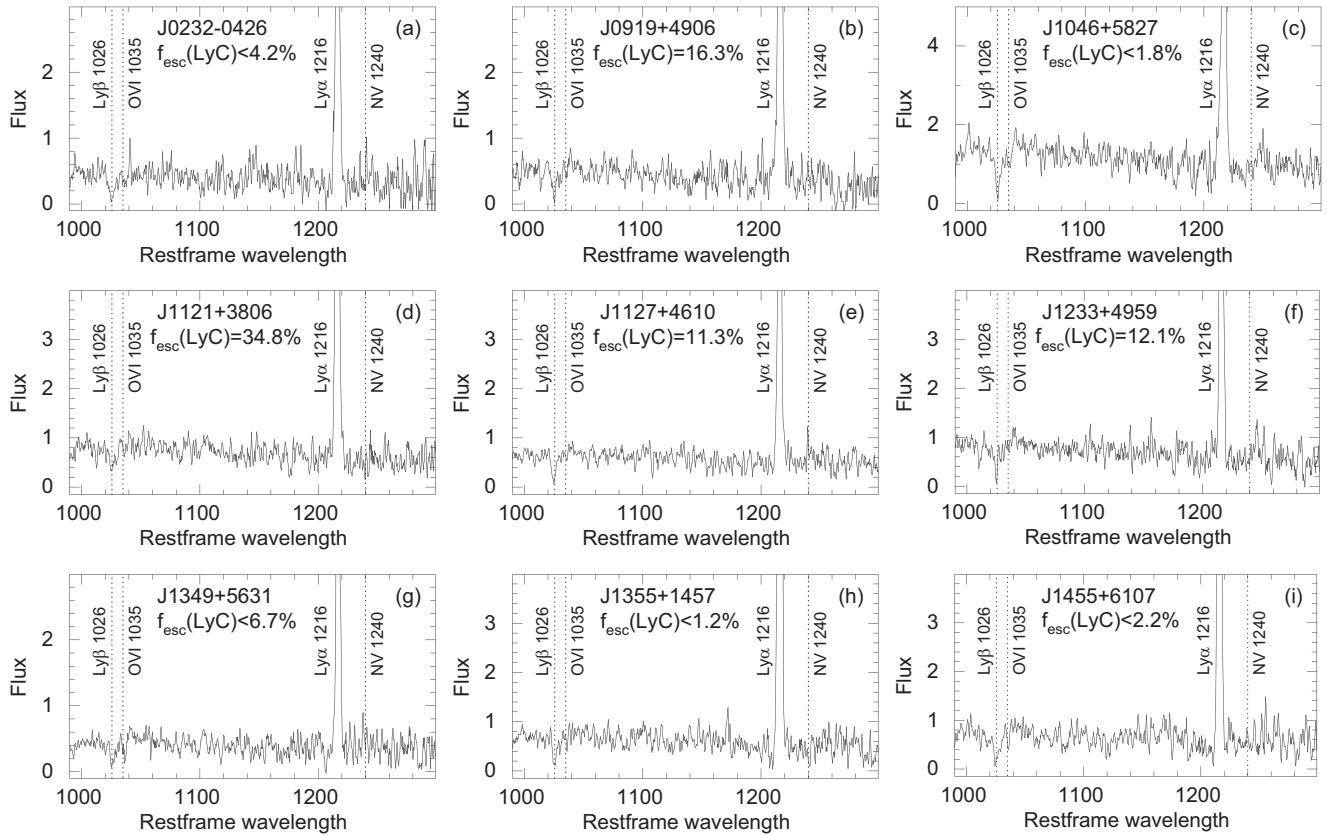**Figure 9.** Segments of COS G140L spectra showing the wavelength regions of the broad stellar lines O VI λ1035 Å and N V λ1240 Å for all LyC leaker candidates studied in this paper. The centres of these lines and of the Ly β line are indicated by vertical dotted lines. Fluxes are in 10^{-16} erg s^{-1} cm^{-2} Å^{-1}, wavelengths are in Å.

f_{esc}(LyC) < 1.8 per cent, < 6.7 per cent, and 12.1 per cent, respectively.

The spectral differences between the galaxies studied by Izotov et al. (2016a,b, 2018a,b) and in this paper could be caused by the lower stellar masses of the present sample. Stellar winds are less likely in low-metallicity massive stars with more transparent interiors. Furthermore, it is possible that there is a fundamental difference in the formation of the most massive stars in galaxies with different stellar masses. The O VI 1035 Å spectral feature arises from the stellar winds in the most massive stars. The left-hand panel of Fig. 10 shows the O VI profile for two STARBURST99 stellar populations (Leitherer et al. 2010) with metallicities of 0.2 $Z_\odot$ (similar to the median gas-phase metallicity of this sample) and 0.05 $Z_\odot$. This O VI 1035 Å profile takes on a classic P-Cygni feature with blueshifted absorption and redshifted emission for very young stellar populations. While the O VI absorption is slightly metallicity-dependent, the redshifted emission profile is nearly constant at these metallicities and fixed ages.

However, the right-hand panel of Fig. 10 shows the extreme sensitivity of the O VI profile to stellar population age (or equivalently the upper end of the IMF), where O VI emission disappears (equal to the grey dashed line) for stellar populations with ages greater than 4 Myr, once stars with masses greater than 60 $M_\odot$ move off the main-sequence (Meynet et al. 1994), or for younger stellar populations with upper stellar mass truncated at $\leq 60 M_\odot$. The stark lack of O VI emission in the observed stellar populations implies that these low $M_\star$ galaxies do not likely have the most massive stars (>60 $M_\odot$). This

could arise from slightly older stellar populations than the previous sample, the IMF of the lower mass sample may not be sufficiently populated, or the O VI profile may not be fully formed in these stellar populations. Thus, high LyC leakage is not necessarily linked to the presence of O VI λ1035 Å emission, as in the case of J1121+3806.

9 CONCLUSIONS

We present new *Hubble Space Telescope* (*HST*) Cosmic Origins Spectrograph (COS) observations of nine compact SFGs, with low stellar masses $M_\star \lesssim 10^8 M_\odot$ and in the redshift range $z = 0.3179$–0.4524. We use these data to study the Ly α emission and the escaping Lyman continuum (LyC) radiation of these SFGs. This study is an extension of the work reported earlier in Izotov et al. (2016a,b, 2018a,b). Our main results are summarized as follows:

1. Emission of Lyman continuum radiation is detected in four out of the nine galaxies with the escape fraction f_{esc}(LyC) in the range between 11 ± 4 per cent (J1127+4610) and 35 ± 6 per cent (J1121+3806). Only upper limits of f_{esc}(LyC) between ~1 and ~7 per cent are obtained for the remaining five galaxies.

2. A Ly α emission line with two peaks is observed in the spectra of seven galaxies, whereas the Ly α profile in one galaxy, J1127+4610, may show more than two peaks, but the S/N ~ 5 even in undersampled spectra is too low to definitely determine that. The signal-to-noise ratio of the J0232−0426 spectrum is also too low to make definite conclusions about the shape of Ly α. The flux minimum between the
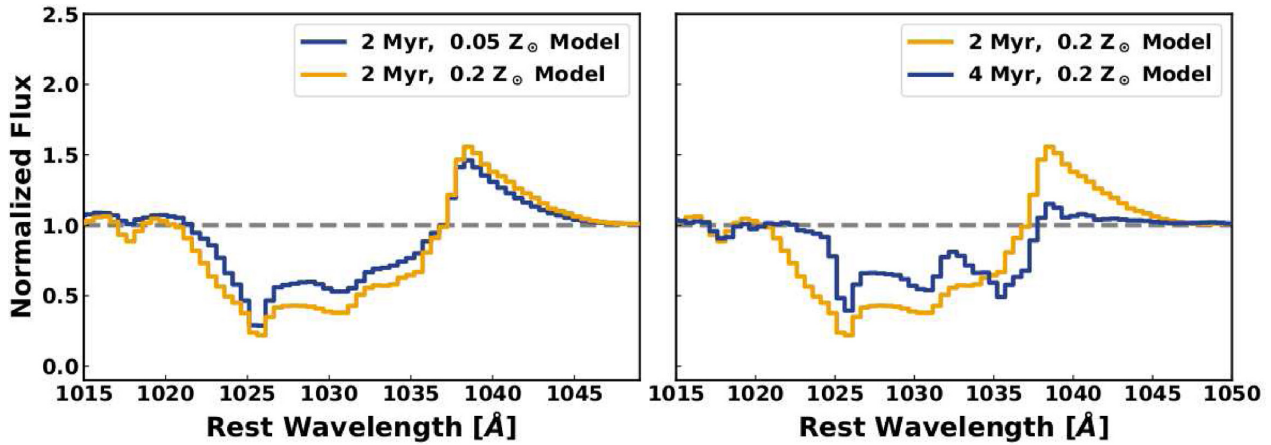
Figure 10. Modelled O VI λ1035 Å line profiles for two STARBURST99 stellar populations (Leitherer et al. 2010) with metallicities of 0.2 Z$_\odot$ and 0.05 Z$_\odot$ (left-hand panel) and with two different starburst ages (right-hand panel).

two peaks approaches the zero value in eight galaxies. However, the flux between the peaks of one galaxy, J1121+3806, with the highest f_{esc}(LyC), is far above the zero value indicating that a considerable fraction of its Ly α emission escaped through low-density ionized channels (holes) in the neutral ISM along the line of sight. A strong anticorrelation between f_{esc}(LyC) and the peak velocity separation V_{sep} of the Ly α profile is found, confirming the finding of Izotov et al. (2018b) and making V_{sep} the most robust indirect indicator of Lyman continuum radiation leakage.

3. Other characteristics such as O$_{32}$ ratio, f_{esc}(Ly α) and the stellar mass $M_\star$ show weak or no correlations with f_{esc}(LyC), with a high spread of values. In particular, our new observations of low-mass LyC leaker candidates, with $M_\star < 10^8$ M$_\odot$, do not confirm the slight trend of increasing f_{esc}(LyC) with decreasing $M_\star$ found by Izotov et al. (2018b) for LyC leakers with higher stellar masses.

4. A bright compact star-forming region (with the exception of J0232−0426, which shows several knots of star formation) superimposed on a low-surface-brightness component, is seen in the COS near ultraviolet (NUV) acquisition images of all eight galaxies (one image is missing due to technical problems). The surface brightness at the outskirts of our galaxies can be approximated by an exponential disc, with a scale length of ~0.34–0.59 kpc. This is ~4 times lower than the scale lengths of the LyC leakers observed by Izotov et al. (2016a,b, 2018a,b), indicating that our new LyC candidates have much lower masses. However, part of this difference may be explained by acquisition exposure times that are ~1.5 times lower for the present sample, resulting in less deep images.

5. The star formation rates in the range SFR ~4 − 14 M$_\odot$ yr^{-1} of our low-mass galaxies, with stellar masses $M_\star < 10^8$ M$_\odot$, are several times lower than those in the LyC leakers studied by Izotov et al. (2016a,b, 2018a,b). However, their specific star formation rates of > 150 Gyr^{-1} are higher than those found in low-redshift LyC leakers. The metallicities of our new galaxies, ranging from $12 + \log$O/H $= 7.77$ to 8.11, are similar to those for LyC leakers studied by Izotov et al. (2016a,b, 2018a,b).

6. At variance with the LyC leakers studied by Izotov et al. (2016a,b, 2018a,b), the O VI λ1035 Å line is not seen in the spectra of our low-mass galaxies. These spectral differences can be caused by the lower stellar masses and lower metallicities of the galaxies in the present sample. The absence of the O VI λ1035 Å line implies that these galaxies do not contain the most massive stars.

DATA AVAILABILITY

The data underlying this article will be shared on reasonable request to the corresponding author.

REFERENCES

Ade P. A. R. et al., 2014, A&A, 571, A16
Aller L. H., 1984, Physics of Thermal Gaseous Nebulae. Reidel Dordrecht
Bian F., Fan X., McGreer I., Cai Z., Jiang L., 2017, ApJ, 837, 12
Borthakur S., Heckman T. M., Leitherer C., Overzier R. A., 2014, Science, 346, 216
Bouwens R. J., Illingworth G. D., Oesch P. A., Caruana J., Holwerda B., Smit R., Wilkins S., 2015, ApJ, 811, 140

Bouwens R. J., Illingworth G. D., Oesch P. A., Atek H., Lam D., Stefanon M., 2017, ApJ, 843, 41

Cardamone C. et al., 2009, MNRAS, 399, 1191

Cardelli J. A., Clayton G. C., Mathis J. S., 1989, ApJ, 345, 245

Caruana J. et al., 2018, MNRAS, 473, 30

Chisholm J. et al., 2018, A&A, 616, 30

Chisholm J., Orlitová I., Schaerer D., Verhamme A., Worseck G., Izotov Y. I., Thuan T. X., Guseva N. G., 2017, A&A, 605, A67

Chisholm J., Prochaska J. X., Schaerer D., Gazagnes S., Henry A., 2020, MNRAS, 498, 2554

Cowie L. L., Barger A. J., Trouille L., 2009, ApJ, 692, 1476

Curtis-Lake E. et al., 2016, MNRAS, 457, 440

de Barros S. et al., 2016, A&A, 585, A51

de Barros S., Oesch P. A., Labbé I., Stefanon M., González V., Smit R., Bouwens R. J., Illingworth G. D., 2019, MNRAS, 489, 2355

Dijkstra M., Gronke M., Venkatesan A., 2016, ApJ, 828, 71

Dressler A., Henry A., Martin C. L., Sawicki M., McCarthy P., Villaneuva E., 2015, ApJ, 806, 19

Endsley R., Stark D. P., Chevallard J., Charlot S., 2021, MNRAS, 500, 5229

Faisst A. L., 2016, ApJ, 829, 99

Finkelstein S. L. et al., 2019, ApJ, 879, 36

Fischer W. J. et al., 2018, Cosmic Origins Spectrograph Instrument Handbook, Version 10.0. STScI, Baltimore

Fletcher T. J., Tang M., Robertson B. E., Nakajima K., Ellis R. S., Stark D. P., Inoue A., 2019, ApJ, 878, 87

Gazagnes S., Chisholm J., Schaerer D., Verhamme A., Rigby J. R., Bayliss M., 2018, A&A, 616, 29

Gazagnes S., Chisholm J., Schaerer D., Verhamme A., Izotov Y., 2020, A&A, 639, 85

Girardi L., Bressan A., Bertelli G., Chiosi C., 2000, A&AS, 141, 371

Grazian A. et al., 2016, A&A, 585, A48

Guseva N. G., Izotov Y. I., Fricke K. J., Henkel C., 2013, A&A, 555, A90

Harikane Y. et al., 2018, ApJ, 859, 84

Hashimoto T. et al., 2017, A&A, 608, 10

Hassan S., Davé R., Mitra S., Finlator K., Ciardi B., Santos M. G., 2018, MNRAS, 473, 227

Hayes M. J., Runnholm A., Gronke M., Scarlata C., 2021, ApJ, 908, 36

Henry A., Scarlata C., Martin C. S., Erb D., 2015, ApJ, 809, 19

Henry A., Berg D. A., Scarlata C., Verhamme A., Erb D., 2018, ApJ, 855, 96

Inoue A. K., Shimizu I., Iwata I., Tanaka M., 2014, MNRAS, 442, 1805

Iwata I. et al., 2009, ApJ, 692, 1287

Izotov Y. I., Thuan T. X., Lipovetsky V. A., 1994, ApJ, 435, 647

Izotov Y. I., Stasińska G., Meynet G., Guseva N. G., Thuan T. X., 2006, A&A, 448, 955

Izotov Y. I., Guseva N. G., Thuan T. X., 2011, ApJ, 728, 161

Izotov Y. I., Guseva N. G., Fricke K. J., Henkel C., 2015, MNRAS, 451, 2251

Izotov Y. I., Orlitová I., Schaerer D., Thuan T. X., Verhamme A., Guseva N. G., Worseck G., 2016a, Nature, 529, 178

Izotov Y. I., Schaerer D., Thuan T. X., Worseck G., Guseva N. G., Orlitová I., Verhamme A., 2016b, MNRAS, 461, 3683

Izotov Y. I., Schaerer D., Worseck G., Guseva N. G., Thuan T. X., Verhamme A., Orlitová I., Fricke K. J, 2018a, MNRAS, 474, 4514

Izotov Y. I., Worseck G., Schaerer D., Guseva N. G., Thuan T. X., Fricke K. J., Verhamme A., Orlitová I., 2018b, MNRAS, 478, 4851

Izotov Y. I., Thuan T. X., Guseva N. G., Liss S. E., 2018c, MNRAS, 473, 1956

Izotov Y. I., Schaerer D., Worseck G., Verhamme A., Guseva N. G., Thuan T. X., Orlitová I., Fricke K. J., 2020, MNRAS, 491, 468

Jaskot A. E., Oey M. S., 2013, ApJ, 766, 91

Jaskot A. E., Oey M. S., 2014, ApJ, 791, L19

Jaskot A. E., Oey M. S., Scarlata C., Dowd T., 2017, ApJ, 851, L9

Jiang L. et al., 2018, ApJ, 772, 99

Kennicutt R. C., Jr, 1998, ARA&A, 36, 189

Khaire V., Srianand R., Choudhury T. R., Gaikwad P., 2016, MNRAS, 457, 4051

Kim K., Malhotra S., Rhoads J. E., Butler N. R., Yang H., 2020, ApJ, 893, 134

Kulkarni G., Worseck G., Hennawi J. F., 2019, MNRAS, 488, 1035

Labbé I. et al., 2013, ApJ, 777, L19

Leitet E., Bergvall N., Hayes M., Linné S., Zackrisson E., 2013, A&A, 553, A106

Leitherer C., Ortiz Otálvaro P. A., Bresolin F., Kudritzki R.-P., Lo Faro B., Pauldrach A. W. A., Pettini M., Rix S. A., 2010, ApJS, 189, 309

Leitherer C., Hernandez S., Lee J. C., Oey M. S., 2016, ApJ, 823, L64

Lejeune T., Buser R., Cuisinier F., 1997, A&AS, 125, 229

Lewis J. S. W. et al., 2020, MNRAS, 496, 4342

Madau P., Haardt F., 2015, ApJ, 813, L8

Marchi F. et al., 2017, A&A, 601, 73

Marchi F. et al., 2018, A&A, 614, 11

Matsuoka Y. et al., 2018, ApJ, 869, 150

Matthee J., Sobral D., Darvish B., Santos S., Mobasher B., Paulino-Afonso A., Röttgering H., Alegre L., 2017, MNRAS, 472, 772

Matthee J., Sobral D., Gronke M., Paulino-Afonso A., Stefanon M., Röttgering H., 2018, A&A, 619, 136

McKinney J. H., Jaskot A. E., Oey M. S., Yun M. S., Dowd T., Lowenthal J. D., 2019, ApJ, 874, 52

Meštric U. et al., 2020, MNRAS, 494, 4986

Meyer R. A. et al., 2020, *MNRAS*, 494, 1560

Meyer R. A., Laporte N., Ellis R. S., Verhamme A., Garel T., 2021, MNRAS, 500, 558

Meynet G., Maeder A., Schaller G., Schaerer D., Charbonnel C., 1994, A&AS, 103, 97

Mitra S., Ferrara A., Choudhury T. R., 2013, MNRAS, 428, L1

Mitra S., Choudhury T. R., Ferrara A., 2018, MNRAS, 473, 1416

Naidu R. P., Tacchella S., Mason C. A., Bose S., Oesch P. A., Conroy C., 2020, ApJ, 892, 109

Nakajima K., Ouchi M., 2014, MNRAS, 442, 900

Nakajima K., Fletcher T., Ellis R. S., Robertson B. E., Iwata I., 2018, MNRAS, 477, 2098

Nakajima K., Ellis R. S., Robertson B. E., Tang M., Stark D. P., 2020, ApJ, 889, 161

Ouchi M. et al., 2008, ApJS, 176, 301

Ouchi M. et al., 2009, ApJ, 706, 1136

Paulino-Afonso A. et al., 2018, MNRAS, 476, 5479

Pentericci L. et al., 2018, A&A, 619, 147x`

Rivera-Thorsen T. E. et al., 2019, Science, 366, 738

Robertson B. E. et al., 2013, ApJ, 768, 71

Robertson B. E., Ellis R. S., Furlanetto S. R., Dunlop J. S., 2015, ApJ, 802, L19

Saha K. et al., 2020, Nat. Astron., 4, 1185

Schmutz W., Leitherer C., Gruenwald R., 1992, PASP, 104, 1164

Shapley A. E., Steidel C. C., Strom A. L., Bogosavljević M., Reddy N. A., Siana B. Mostardi R. E., Rudie G. C., 2016, ApJ, 826, L24

Shen X., Hopkins P. F., Faucher-Giguére C.-A., Alexander D. M., Richards G. T., Ross N. P., Hickox R. C., 2020, MNRAS, 495, 3252

Smit R. et al., 2014, ApJ, 784, 58

Sobral D. et al., 2018, MNRAS, 477, 2817

Stark D. P., 2016, ARA&A, 54, 761

Stasińska G., Izotov Y., Morisset C., Guseva N., 2015, A&A, 576, A83

Steidel C. C., Pettini M., Adelberger K. L., 2011, ApJ, 546, 665

Steidel C. C., Bogosavljević M., Shapley A. E., Reddy N. A., Rudie G. C., Pettini M., Trainor R. F., Strom A. L., 2018, ApJ, 869, 123

Thuan T. X., Martin G. E., 1981, ApJ, 247, 823

Trebitsch M., Blaizot J., Rosdahl J., Devriendt J., Slyz A., 2017, MNRAS, 470, 224

Vanzella E. et al., 2010, ApJ, 725, 1011

Vanzella E. et al., 2012, ApJ, 751, 70

Vanzella E. et al., 2015, A&A, 576, A116

Vanzella E. et al., 2018, MNRAS, 476, L15

Vanzella E. et al., 2020, MNRAS, 491, 1093

Verhamme A., Orlitová I., Schaerer D., Hayes M., 2015, A&A, 578, A7

Verhamme A., Orlitová I., Schaerer D., Izotov Y., Worseck G., Thuan T. X., Guseva N., 2017, A&A, 597, A13

Vielfaure J.-B. et al., 2020, A&A, 640, 30

Wang F. et al., 2019, ApJ, 884, 30

Wise J. H., Cen R., 2009, ApJ, 693, 984

Wise J. H., Demchenko V. G., Halicek M. T., Norman M. L., Turk M. J., Abel T., Smith B. D., 2014, MNRAS, 442, 2560

Worseck G., Prochaska J. X., Hennawi J. F., McQuinn M., 2016, ApJ, 825, 144

Wright E. L., 2006, PASP, 118, 1711

Yajima H., Choi J.-H., Nagamine K., 2011, MNRAS, 412, 411

Yang H. et al., 2017a, ApJ, 844, 171

Yang H., Malhotra S., Rhoads J. E., Leitherer C., Wofford A., Jiang T., Wang J., 2017b, ApJ, 847, 38

This paper has been typeset from a TEX/LATEX file prepared by the author.